Towards Identification of Progressive Damage in Structures under Non-stationary Excitation

by

Peter Friesen

A thesis

presented to Lakehead University

in fulfillment of the

thesis requirement for the degree of

Master of Science

in

Civil Engineering

Thunder Bay, Ontario, Canada, 2017

© Peter Friesen 2017

Abstract

Monitoring and retrofitting of large-scale infrastructure is of paramount importance specially when they are subjected to natural hazards like strong wind, severe earthquakes or man-made excitation. Once the rich vibration data is collected from the structures, a robust system identification method is required to extract the hidden structural information, and undertake necessary condition assessment and rehabilitation. Most of the traditional modal identification methods are reliant on stationarity assumption of the vibration response and posed difficulty while analyzing nonstationary vibration occurred due to natural hazards. Apart from the excitation-induced nonstationarity, the inherent damages in the structure also cause frequency-dependent nonstationarity in the response. With such combination of both amplitude and frequency-dependent nonstationary response, the modal identification becomes a significantly challenging task.

Recently tensor decomposition based methods are emerged as powerful and yet generic blind (i.e. without requiring a knowledge of input characteristics) signal decomposition tool for structural modal identification. In this thesis, a tensor decomposition based system identification method is further explored to estimate modal parameters using amplitude-dependent nonstationary vibration generated due to either earthquake or pedestrian induced excitation in a structure. The effects of lag parameters and sensor densities on tensor decomposition are studied with respect to the extent of nonstationarity of the responses characterized by the stationary duration and peak ground acceleration of the earthquake. A suite of more than 1400 earthquakes is used to investigate the performance of the proposed method under a wide variety of ground motions utilizing both complete and partial measurements of a high-rise building model. Apart from the earthquake, human-induced nonstationary vibration of a real-life pedestrian bridge is also used to verify the accuracy of the proposed method.

i

Once the method is verified using amplitude-based nonstationary response, Cauchy continuous wavelet transform is integrated with the tensor decomposition to track time-varying characteristics of each modal responses and detect the progressive damage. With such an integrated framework, the proposed method is able to identify both amplitude and frequency-dependent nonstationary responses. The proposed technique is validated using a suite of numerical studies as well as a laboratory experiment where the progressive damage is simulated in the structural component with a heating torch.

Acknowledgements

I would like to express my sincere gratitude to my advisor Dr. Ayan Sadhu for his valuable support and encouragement during my graduate studies. His patience, guidance and timely feedback were of great help throughout my research and thesis. This thesis would not have been possible without the support and mentorship of Dr. Sadhu.

I would also extend my warmest thanks to my thesis committee members, Dr. Sam Salem and Dr. Kefu Liu, for their comments and valuable feedback.

I would like to thank my colleagues Mr. Mohamed Barbosh, Ms. Miao Yuan, and Mr. Yu Zhang for their countless discussion and assistance in my laboratory experiments. I would also thank several undergraduate degree-project students who were involved in the collection of research data. Special thanks are reserved to Mr. Conrad Hagstrom (the laboratory manager of Civil Engineering department at Lakehead University) for his kind technical assistance to set up the experiments.

I gratefully acknowledge the funding provided by the Natural Sciences Engineering Research Council of Canada (NSERC) and Lakehead University to undertake this work.

Finally, I would like to thank my wife Renata, kids, and my parents for their sacrifice, emotional support and love throughout the process and completion of my Master's degree at Lakehead.

Dedication

This thesis is dedicated to my wife Ranata and daughters Janiya and Zimra.

Table of Contents

List of Tables

List of Figures

Abbreviations

CCWT Cauchy continuous wavelet transform 47–50, 53–57, 60

CWT Continuous wavelet transform 47–49

DOF Degrees of freedom 16, 18, 20, 29, 49, 53, 55, 57, 60

FFT Fast Fourier transform 23

PARAFAC Parallel factor 10–12, 14, 15, 18–21, 23, 25, 29, 47, 48, 53, 57, 60

SHM Structural health monitoring 1–3, 18, 49

SSI Stochastic subspace identification 38

Chapter 1

Introduction

1.1 Overview

As buildings, bridges and many other large civil infrastructure age, they undergo a wide range of excitation including strong winds, earthquake or man-made hazard. Such time-varying and nonstationary external loads cause significant deterioration in civil structures. A structure that experiences minor damage under operational load may still be considered structurally sound. However, initial damage may progressively worsen over time that increases the possibility of catastrophic failure in the near future. Therefore, continuous monitoring and inspection of the structure is important to prevent any major failure later. The motivation of this thesis is to develop a vibration-based damage detection technique capable of identifying progressive damage in structures under nonstationary excitation.

In general, monitoring large structures using manual and visual inspection are costly, time consuming and inaccurate. The emergence of Structural health monitoring (SHM) provides an effective method of damage detection through the collection of output measure-
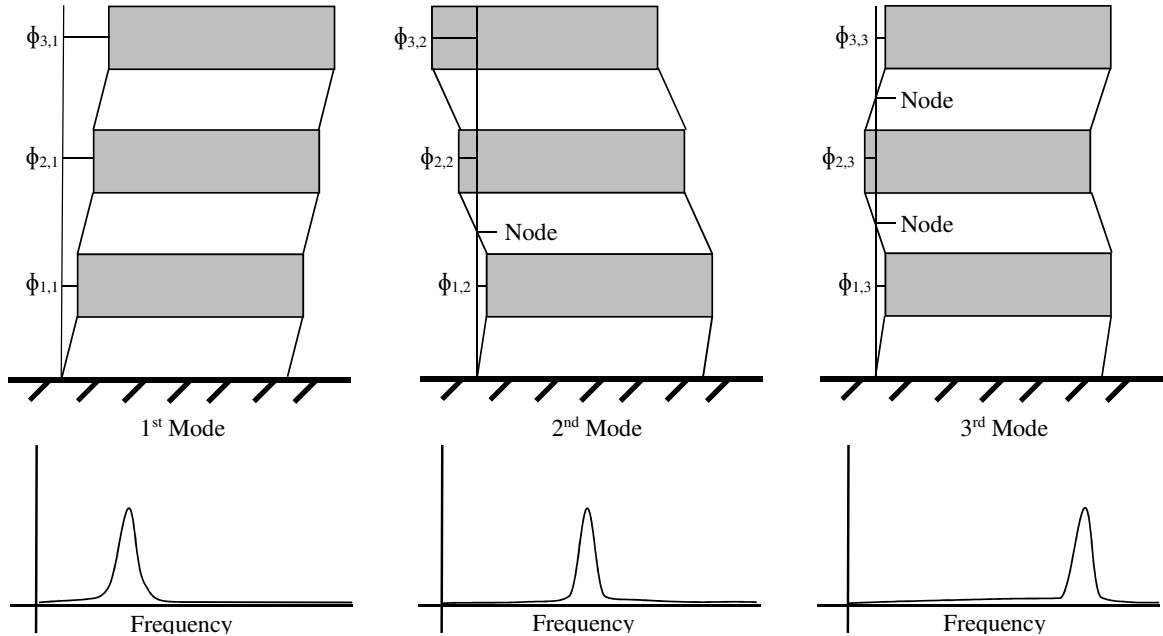
Figure 1.1: Idealized modal parameters of a three-story building

ments. Vibration-based SHM methods [5] are very powerful to detect local as well as global damage that cannot be identified using traditional methods. Modal identification [35] is one of the key components of SHM where modal parameters (i.e, damping, frequency, and modeshapes as shown in Fig. 1.1) are extracted directly from vibration measurements. The central idea of these techniques is that structural damage causes changes in these modal parameters and the proposed method should be able to track these changes. Development of modal identification techniques was initiated as input-output methods in the 1970s. However, due to the lack of input measurements and the associated cost, "output-only" methods (i.e. blind identification) are more suitable to large-scale civil structures.

While many SHM techniques have been studied considering detection of discrete dam-

age, there has been a limited amount of research towards detection of progressive damage of structures that may occur due to natural hazards such as strong winds and earthquakes that are nonstationary in nature. This research is intended to explore a robust damage detection technique for structures with progressive damage resulting due to such nonstationary excitation.

1.2 Literature Review

The SHM is primarily consisted of four key elements: data sensing, data acquisition, system identification and decision making. Over past few decades, the topic of SHM has seen significant advancement in newer system identification techniques addressing a wide range of challenging situations of large-scale structures. However, despite all the advancements in signal processing, progressive damage detection of structures remains a challenge. In this section, a detailed literature review on recent damage detection methods is presented.

Since 1970, different modal identification techniques have been developed towards various SHM applications. These techniques fall under five categories; time or frequency domain, time-frequency domain, pattern recognition or hybrid methods. A current review paper [5] of signal processing techniques provides an excellent summary of advantages and disadvantages of different signal processing techniques.

1.2.1 Time-domain Methods

Time domain methods were among the preliminary methods of the SHM techniques. Ma et. al. [34] used vibration data to track the changes in stiffness. However, they concluded that noise contamination, as well as environmental changes affect the performance of the

method to detect small variations in stiffness. Jang et al. [23] employed stochastic dynamic damage locating vector (SDDLV) method that tracks the dynamic flexibility matrices. [6] investigated normalized curvature difference of waveform jerk energy [6] and the curvature difference to find the location. In a different study, an autoregressive model [38] with a hidden Markov model was used to determine the probabilistic progressive damage of a structure. In [10], an optimization approach was adopted that minimized the error between the moment generating function and a numerical modal of the structure to identify damage. This method can be applied using limited sensors, but required significant user intervention. Zhong and Chang [59] applied recursive subspace identification to recognize structural changes under non-stationary excitation. Liu et al. [33] extended the random decrement technique under non-stationary structural response. In summary, time domain methods are easier to implement, however most of them require input data which is difficult to obtain in large structures and have shown poor performance towards progressive damage detection.

1.2.2 Frequency-domain Methods

Frequency domain analysis converts a time history into its frequency spectrum which allows the user to see the frequencies that are present within the system. Valdes-Gonzalez et al. [55] used to detect changes in stiffness of the structure using the power spectral density functions of the dynamic strain measurements [52]. Based on frequency domain decomposition [19], the Bayesian approach employing the Markov-chain Monte Carlo method was used to estimate the modal parameters. In [21], l1-norm of the algebric difference between damaged and undamaged structures was used to localize and quantify damage. In another study, the problem of system identification with incomplete structural information was

addressed by [16]. One of the major drawbacks of frequency domain analysis is that it is not possible to determine the span of time in which frequency changes occur, which is critical to detect progressive damage correctly.

1.2.3   Time-frequency Methods

Time-frequency analysis gives a better picture of the frequency change within a system in conjunction with time. A statistical method based on wavelet packet transform [51] was developed for SHM under pulse loading. This method analyzed acceleration time histories which were decomposed into wavelet coefficients and subsequently the dominant energies are extracted and quantified. Sadhu and Hazra [44] combined blind source separation (BSS) with time-series model that estimated the modal response through the BSS and then the time-series model predicted the next measurement step. Consequently, damage location, severity and damage instant were identified. A recursive least squares (RLS) algorithm [26] in combination with adaptive wavelet filtration was used for non-stationary systems as it adjusted the wavelet to reflect the changes in the system. Adaptive wavelet filtration matched the wavelet filter characteristics to the frequency at the time, allowing for better tracking of damage. This technique reduced the computation time and increased the convergence speed of the RLS algorithm. Using spectrogram representation of short-time-Fourier transform, [3] came up with an optimal bias-compensated estimator to remove some of the time-frequency distortions through correction curves developed via Monte Carlo simulations. Musafere et al. [40] proposed an integrated second-order blind separation (SOBI) with time-variant auto-regressive (TVAR) model to conduct discrete damage detection. In this method, the SOBI was used to identify the modal responses and then TVAR model tracked the modal changes to identify severity and instant of discrete

damage.

Wavelet-based [17] based frequency response function was developed to detect abrupt changes in a time-variant system. [54] used two signal processing steps where the signal was first processed through continuous wavelet transformation (CWT) followed by the generalized discrete Teager-Kaiser energy operator that localized and magnified the damaged modeshapes. A recent method [12] applying joint approximate diagonalization of the power spectral density matrices also yielded the operational deflection shapes of the structure. This method was then compared with several dominant characteristic deflection shapes at different natural frequencies to create a damage index. In summary, time-frequency methods are promising for detecting progressive damage owing to their time-varying frequency decomposition capability. However, these methods have not been explored under nonstationary excitation.

1.2.4 Pattern Recognition Methods

Pattern recognition methods employ statistical analysis and novelty detection approaches to distinguish changes in the system parameters of the structure. For example, the AR-Markov models [15] are designed from input/output measurement of the system and attempted to determine the extent of damage within a member. Panigrahi et al. [41] used residual force vector analysis along with genetic algorithm to detect the location and extent of damage in multi-storied structure. Research by Khoa et al. [24] tested three methods of dimensional reduction: random projection, principal component analysis, and support vector machine. On the other hand, Link and Zimmerman [32] explored orthogonal matching pursuit to find the level of damage from frequency response functions. In [49], three dynamic signatures including modeshape curvature, modal strain energy and modal flexi-

bility matrix were extracted to assess structural damage. Using a curve fitting technique, the aforementioned dynamic signatures were compared to a baseline structure for probabilistic damage identification. Another novelty detection method, namely self-organizing maps [4], was able to quantify and locate reduction in member stiffness. They found this method to be effective with up to 10% measurement noise.

1.2.5 Hybrid Methods

This class of techniques uses a combination of several signal decomposition techniques. For example, [25] combined discrete wavelet transform (DWT) with autoregressive moving average models and support vector machines (SVM) to perform global damage detection in smart structures equipped with magnetorheological damper under earthquake excitation. Arsava et al. [9] also used the DWT with relevance vector machine (RVM), a Bayesian extension of SVM, and found that the RVM had a faster training process with similar accuracy to the SVM. Multi-class non-linear RVM was developed for damage detection of non-linear systems with random excitation. A method combining [58] structural damage prognosis with fuzzy C-means clustering was used to identify the type of linear and nonlinear damage of structures. In another study, a new recursive stochastic subspace identification [57] was developed where the Hankel matrix of the data was continuously updated with new data. Recently, Su et al. [50] developed a two-step process for identifying the location of damage. The method used continuous Cauchy wavelet transform for modal identification followed by damage locating vectors applied to the identified flexibility matrix.

1.3 Gap Areas

With above review of the existing literature, the following gap areas are identified that could be considered to improve the state-of-the-art damage detection methods.

- Time-frequency methods have better potential to perform modal identification of time-varying systems. However, there has been limited research in this area when the structure is excited by nonstationary excitation. Such amplitude-dependent non-stationarity is an important factor to be considered in the system identification stage due to the presence of strong winds and severe earthquakes affecting the structures.

- There has been significant research in identifying discrete damage. However, very few research has been conducted in the area of progressive damage to address the frequency-dependent nonstationary.

- Adequate and realistic validation of the damage detection method is also very critical while developing a new method. Moreover, it would be worth to investigate the effect of limited number of sensors.

1.4 Thesis Objectives

Based on the above gap areas, the following objectives are considered in this thesis.

1. Explore a newer time-frequency system identification method that can identify modal parameters using amplitude-dependent nonstationary response of the structures.

    (a) Investigate the effect of user-defined parameters of the proposed method.

(b) Evaluate the performance of tensor decomposition using a suite of nonstationary excitation including earthquake as well human-induced vibration.

(c) Evaluate the effect of limited number of sensors.

2. Once the above methodology is successfully explored, develop a robust damage detection technique that can accurately identify the progressive damage in a structure subjected to nonstatioary excitation.

3. Validate the proposed method using a suite of numerical and experimental studies.

Chapter 2

Tensor Decomposition Method

In this chapter a new time-frequency method, called tensor decomposition, is explored to estimate modal parameters of structures using nonstationary vibration response. Tensor decomposition is a powerful blind system identification method that does not require knowledge of input data. This method involves several factors including lag parameters and limited number of sensors that will be studied in the context of stationary and amplitude-dependent nonstationary excitation.

2.1 Introduction

In recent years, PARAllel FACtor (also known as Parallel factor (PARAFAC) decomposition) or tensor decomposition method has emerged as a powerful modal identification technique [45]. In this chapter, the performance of PARAFAC decomposition is explored under a wide range of earthquake-induced vibration that are associated with amplitude-dependent nonstationary.

In this method, a tensor is built from the covariance matrix of sensor vibration data under a set of multiple lags. This covariance tensor is decomposed into covariances of the modal responces using a multi-linear algebra method known as alternating least squares (ALS) [48, 37]. Using canonical decomposition [13] and parallel factor analysis [20], the matricization operation perform signal decomposition using both complete as well as partial measurement cases. Antoni and Chauhan [7] used alternating least squares (ALS) to solve tensor decomposition associated with modal identification using a limited number of sensors [42]. The underdetermined signal separation capability of PARAFAC decomposition was recently explored to identify the modal parameters of high-rise building [1, 36, 2] and a structure equipped with tuned-mass damper [46] using limited sensor measurements.

In the case of complete measurement case, the modal responses can be obtained directly from the raw vibration measurements without any post-processing. On the other hand, when only limited sensor measurements are available, PARAFAC decomposition results in the covariance of modal responses from which frequencies and damping are subsequently estimated. Recently, PARAFAC decomposition was integrated with wavelet packet transform (WPT) to improve the source separation capability where mode-mixing in the WPT coefficients was alleviated using PARAFAC decomposition [45, 47]. The rank order selection is one of the prerequisite in this method, which is an impediment for automated system identification. In order to alleviate this, a cluster diagram of modal frequencies is proposed under a suite of multiple rank orders [43] from which the optimal rank order is chosen based on clustered densities of modal parameters. In this process, the effect of spurious modes is also circumvented and the modal frequencies are delineated from the excitation frequencies. However, none of the above studies investigates the performances of PARAFAC decomposition under nonstationary excitation. In this chapter, the PARAFAC decomposition is studied under a wide range of nonstationary vibration due to earthquakes as well as

11

human-induced excitations. The effect of lag parameters is investigated with respect to the extent of nonstationarity in the data. The performance of this method under limited sensor densities is also explored in a high-rise building model and a full-scale pedestrian bridge located in the campus of Lakehead University, Canada.

This chapter is organized as follows. First, the brief literature of PARAFAC decomposition is presented in the introduction section. The background of PARAFAC decomposition is discussed next followed by the mathematical equivalence of tensor decomposition with modal identification. The PARAFAC method is then validated using numerical and real-life case studies in the results section followed by key conclusions.

2.2 Background

A signal may be expressed through a multi-dimensional array. This allows tensor representation and use of multi-liner algebra tool which is more effective than linear algebra tool (e.g. principal component analysis [11, 48]). A vector $\mathbf{s} = s_i \in \Re^{n_1}$ is a first-order tensor, whereas a matrix $\mathbf{S} = s_{ij} \in \Re^{n_1 \times n_2}$ is a second-order tensor. It follows, a zth order tensor is written as:

$$\bar{\mathbf{S}} = s_{ijk...z} \in \Re^{n_1 \times n_2 \times n_3 \times .... \times n_z}. \tag{2.1}$$

To better understand tensors, first take a simple 2x2x2 tensor as shown in Fig. 2.1. Each tensor is comprised of higher order fibres, mode-1 $(t_{:jk})$, mode-2 $(t_{i:k})$, and mode-3 $(t_{ij:})$ fibres. A three-dimensional tensor, separated into three matrices representing each dimension (horizontal, lateral, and in plane) this is known as matricization. A third-order tensor is first seperated into a sum of outer products of triple vectors as seen in Fig. 2.2 [11]:
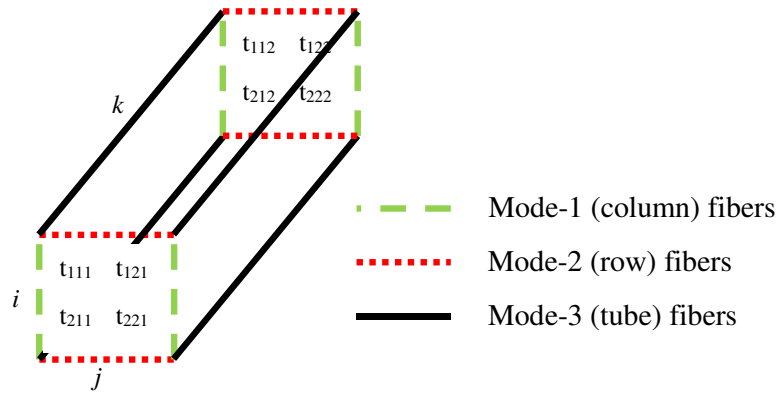
Figure 2.1: Block representation of a 2 x 2 x 2 tensor fibres, t_{ijk}
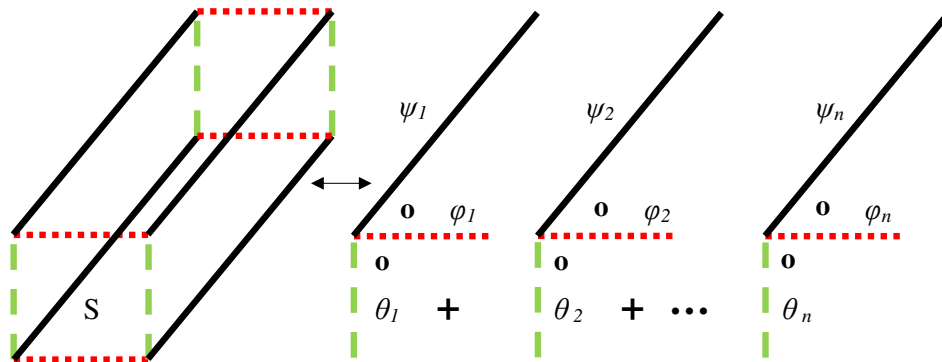
Figure 2.2: Tensor decomposition

13

$$\bar{\mathbf{S}} = \sum_{r=1}^{R} \boldsymbol{\theta}_r \circ \boldsymbol{\phi}_r \circ \boldsymbol{\psi}_r \Longleftrightarrow \bar{S}_{ijk} = \sum_{r=1}^{R} \theta_{ir} \phi_{jr} \psi_{kr} \qquad (2.2)$$

where "$\circ$" denotes outer product with $i \in [1 \ I]$, $j \in [1 \ J]$ and $k \in [1 \ K]$. In Eq. (2.2), R is the number of rank-1 tensors present in $\bar{\mathbf{S}}$. This is also defined as trilinear model of $\bar{\mathbf{S}}$, $\bar{\mathbf{S}} = [\boldsymbol{\Theta}, \boldsymbol{\Phi}, \boldsymbol{\Psi}]$, where the matrices are given by $\boldsymbol{\Theta} = (\boldsymbol{\theta}_1, \boldsymbol{\theta}_2, ..., \boldsymbol{\theta}_R)$, $\boldsymbol{\Phi} = (\boldsymbol{\phi}_1, \boldsymbol{\phi}_2, ..., \boldsymbol{\phi}_R)$, and $\boldsymbol{\Psi} = (\boldsymbol{\psi}_1, \boldsymbol{\psi}_2, ..., \boldsymbol{\psi}_R)$. As shown in Eq. (2.2), each triple vector product is a rank-1 tensor, namely PARAFAC component. Eq. (2.2) represents the summation of R such PARAFAC components that fit the higher order tensor $\bar{\mathbf{S}}$ [11, 28]. The fundamental technique was developed by two different independent research: canonical decomposition (CANDECOMP) [13] and PARAllel FACtor (PARAFAC) analysis [20]. The algorithms can be categorized in three main groups, namely (a) alternating least squares (ALS) (b) derivative-based methods and (c) direct or non-iterative approaches [11]. Out of three methods, the ALS method is the most popular method because of an easier implementation, smooth convergence and robust handling for higher order tensors. The key steps of the ALS are briefly presented in Appendix A. The details of tensor decomposition can be found in the literature [11] and are not repeated for brevity.

A simple demonstration of the signal separation capability of PARAFAC decomposition is considered next. Consider a linear mixtures of three harmonics (sources, s) with frequencies 1.0, 2.5 and 1.2 Hz containing a measurement noise of 20% shown in the first two rows of Fig. 2.3:

14
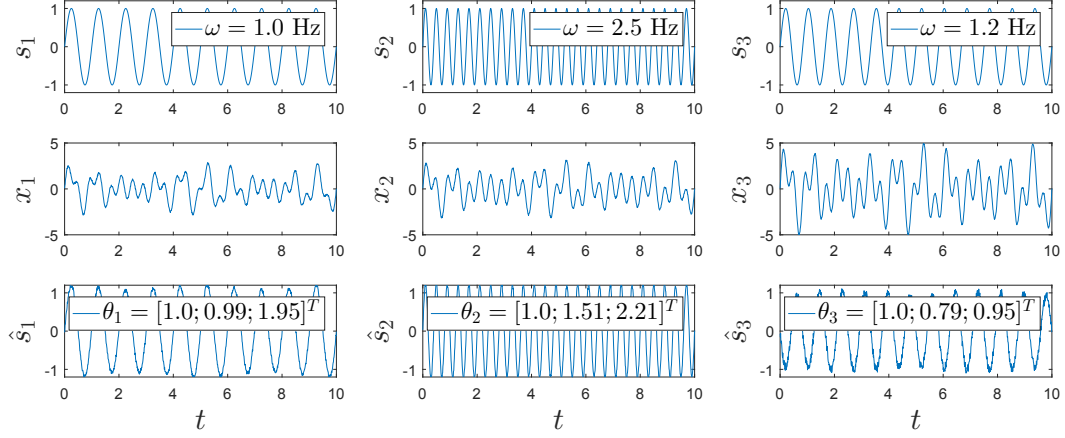
Figure 2.3: Simulated mixtures and corresponding signal separations using the PARAFAC decomposition

$$
\begin{bmatrix} x_1 \\ x_2 \\ x_3 \end{bmatrix} = \begin{bmatrix} 1 & 1 & 1 \\ 1 & 1.5 & 0.8 \\ 2 & 2.2 & 1 \end{bmatrix} \begin{bmatrix} s_1 \\ s_2 \\ s_3 \end{bmatrix}
$$
$$
x = \theta s \tag{2.3}
$$

Since the mixtures contain three sources, rank-3 PARAFAC decomposition (i.e., $R = 3$) is performed over these mixtures to extract three hidden sources. The PARAFAC decomposition yields $\hat{\boldsymbol{\theta}}_1$, $\hat{\boldsymbol{\theta}}_2$ and $\hat{\boldsymbol{\theta}}_3$ as shown in the last row of Fig. 2.3. This yields the mixing matrix by concatenating successive normalized (w.r.t. x_1) $\hat{\boldsymbol{\theta}}$ that is approximately equal to Eq. (2.3):

15

$$\hat{\boldsymbol{\theta}} = \begin{bmatrix} \hat{\theta}_1 & \hat{\theta}_2 & \hat{\theta}_3 \end{bmatrix} = \begin{bmatrix} 0.93 & 0.81 & -0.97 \\ 0.92 & 1.22 & -0.77 \\ 1.82 & 1.79 & -0.92 \end{bmatrix} \Leftrightarrow \hat{\boldsymbol{\theta}} = \begin{bmatrix} 1.0 & 1.0 & 1.0 \\ 0.99 & 1.5 & 0.79 \\ 1.95 & 2.2 & 0.95 \end{bmatrix} \qquad (2.4)$$

2.3   Tensor decomposition-based Modal Identification

In this section, tensor decomposition method is explored for modal identification. A linear, proportionally damped, and discrete lumped-mass system with n_d Degrees of freedom (DOF) when subjected to an excitation force, $\mathbf{P}(t)$ can be expressed as:

$$\mathbf{M}\ddot{\mathbf{y}}(t) + \mathbf{C}\dot{\mathbf{y}}(t) + \mathbf{K}\mathbf{y}(t) = \mathbf{P}(t) \qquad (2.5)$$

where, $\mathbf{y}(t)$ is the displacement vector at the lumped masses. $\mathbf{M}$, $\mathbf{C}$, and $\mathbf{K}$ are the mass, damping and stiffness matrices of the multi-degree-of-freedom system. For example, $\mathbf{P} = \mathbf{M}\mathbf{I}\ddot{\mathbf{u}}_{\mathbf{g}}$ where ground motion (i.e., $\ddot{\mathbf{u}}_{\mathbf{g}}(t)$) is applied at the base. The solution of Eq. (2.5) can be expressed in terms of modal superposition of vibration modes with the following matrix form:

$$\mathbf{y} = \boldsymbol{\Gamma}\mathbf{q} \qquad (2.6)$$

where, $\mathbf{y} \in \Re^{n_y \times N}$ is a matrix consisting of measurements $\mathbf{y}$, $\mathbf{q} \in \Re^{n_d \times N}$ is a matrix of the corresponding modal responses, $\boldsymbol{\Gamma}_{n_y \times n_d}$ is the mode shape matrix, and N is the number of data points in the measurement. n_y is the number of measurement channels.

The covariance matrix $\mathbf{Z}_{\mathbf{y}}(\tau_k)$ of vibration measurements ($\mathbf{y}$) evaluated at time-lag τ_k can be written as:

$$\mathbf{Z}_{\mathbf{y}}(\tau_k) \;=\; E\left\{\mathbf{y}(n)\mathbf{y}^T(n - \tau_k)\right\} = \boldsymbol{\Gamma}\mathbf{Z}_{\mathbf{q}}(\tau_k)\boldsymbol{\Gamma}^T \qquad (2.7)$$

where,

$$\mathbf{Z_q}(\tau_k) = E\left\{\mathbf{q}(n)\mathbf{q}^T(n - \tau_k)\right\}. \tag{2.8}$$

and $\mathbf{q}$ are the hidden sources. Let us consider the following annotations to simplify the mathematical notations of successive derivations,

$$Z_{y_1 y_2}(\tau_k) = Z_{12k}^y \iff Z_{y_i y_j}(\tau_k) = Z_{ijk}^y$$
$$Z_{q_1}(\tau_k) = Z_{k1}^q \iff Z_{q_l}(\tau_k) = Z_{kl}^q. \tag{2.9}$$

Considering a case with three available measurements where $\mathbf{y} = \{y_1, y_2, y_3\}$, Eq. (2.7) with above simplified notations can be represented as follows:

$$\begin{bmatrix} Z_{11k}^y & Z_{12k}^y & Z_{13k}^y \\ Z_{21k}^y & Z_{22k}^y & Z_{23k}^y \\ Z_{31k}^y & Z_{32k}^y & Z_{33k}^y \end{bmatrix} = \begin{bmatrix} \Gamma_{11} & \Gamma_{12} & \Gamma_{13} \\ \Gamma_{21} & \Gamma_{22} & \Gamma_{23} \\ \Gamma_{31} & \Gamma_{32} & \Gamma_{33} \end{bmatrix} \begin{bmatrix} Z_{k1}^q & 0 & 0 \\ 0 & Z_{k2}^q & 0 \\ 0 & 0 & Z_{k3}^q \end{bmatrix} \begin{bmatrix} \Gamma_{11} & \Gamma_{21} & \Gamma_{31} \\ \Gamma_{12} & \Gamma_{22} & \Gamma_{32} \\ \Gamma_{13} & \Gamma_{23} & \Gamma_{33} \end{bmatrix}. \tag{2.10}$$

Eq. (2.10) can now be expressed as:

$$Z_{12k}^y = \Gamma_{11}\Gamma_{21}Z_{k1}^q + \Gamma_{12}\Gamma_{22}Z_{k2}^q + \Gamma_{13}\Gamma_{23}Z_{k3}^q \tag{2.11}$$

which can be generalized for Z_{ijk}^y of Eq. (2.10) as:

$$Z_{ijk}^y = \Gamma_{i1}\Gamma_{j1}Z_{k1}^q + \Gamma_{i2}\Gamma_{j2}Z_{k2}^q + \Gamma_{i3}\Gamma_{j3}Z_{k3}^q = \sum_{r=1}^{3} \Gamma_{ir}\Gamma_{jr}Z_{kr}^q \quad i, j = 1:3; k = 1:K. \tag{2.12}$$

17

For any general n_d-DOF dynamical system, Eq. (2.12) can be simplified as:

$$Z_{ijk}^y = \sum_{r=1}^{n_d} \Gamma_{ir}\Gamma_{jr}Z_{kr}^q \iff \mathbf{Z^y} = \sum_{r=1}^{n_d} \mathbf{\Gamma_r} \circ \mathbf{\Gamma_r} \circ \mathbf{Z_r^q}. \qquad (2.13)$$

Considering the similarity between Eq. (2.2) and Eq. (2.13), it is observed that by decomposing the third order tensor $\mathbf{Z^y}$ into n_d number of PARAFAC components (i.e., modal responses), the mixing matrix (i.e., Γ) can be estimated. By using PARAFAC decomposition of $\mathbf{Z^y}$, the resulting solutions yield the mixing matrix (i.e., modeshape matrix) $\mathbf{\Gamma} = [\mathbf{\Gamma_1}, \mathbf{\Gamma_2}, \mathbf{\Gamma_3}, ..., \mathbf{\Gamma_{n_d}}]$ and the auto-correlation function $\mathbf{Z_r^q}$ for $r = 1, 2, 3, ..., n_d$ from which the natural frequencies and damping of the individual modal responses can be estimated. In this way, the mathematical equivalence of PARAFAC decomposition and modal identification is established [45].

However, the performance of PARAFAC decomposition has not been yet studied under nonstationary vibration. It may be noted that the lag parameter (i.e., K) plays an important role in separating the PARAFAC components. In this chapter, the effect of K is studied under a wide range of nonstationary measurements obtained using more than 1400 ground motions and human-induced vibrations.

One of the most attractive features of PARAFAC decomposition is that it has the ability to perform separation when the rank is higher than the smallest dimension of the tensor [28]. This property of the PARAFAC decomposition can be utilized to solve underdetermined modal identification problems in SHM, where a limited number of sensors is used or there is malfunctioning of the sensors. Comparing Eq. (2.2) and Eq. (2.13), it is observed that Eq. (2.13) is a special case of PARAFAC tensor model with $\phi = \theta$. Hence, a more relaxed uniqueness condition is proposed where the following inequality is satisfied [28]:

$$\frac{n_d(n_d - 1)}{2} = \frac{n_y(n_y - 1)}{4}\left[\frac{n_y(n_y - 1)}{2} + 1\right] - \frac{n_y!}{(n_y - 4)!4!}(n_y)_{\{n_y \geq 4\}} \qquad (2.14)$$

where,

$$(n_y)_{\{n_y \geq 4\}} = 0 \quad n_y < 4$$

$$(n_y)_{\{n_y \geq 4\}} = 1 \quad n_y \geq 4. \qquad (2.15)$$

For a given number of measurements (n_y), an upper bound of source separability for PARAFAC decomposition can be computed using Eq. (2.14) which is tabulated in Table 2.1 where n_d^u is the highest number of PARAFAC components (i.e., modal responses) that can be extracted from n_y measurements.

Table 2.1: Upper bound of source separation capability of PARAFAC decomposition

n_y	2	3	4	5	6	7	8	9	10
n_d^u	2	4	6	10	15	20	26	33	41

Table 2.1 shows that with rank-n_d PARAFAC decompositions of Eq. (2.13), n_d number of sources can be extracted from n_y measurements, when $2 \leq n_d \leq n_d^u$. In this way, one can undertake a straight-forward approach to solve underdetermined modal identification problems, where n_d sources are identified from n_y vibration measurements even when $n_y \leq n_d$. In this chapter, the effect of fewer number sensors (i.e n_y) and their locations are also studied under a wide range of nonstationary measurements.

The main focus of this chapter is to investigate the performance of PARAFAC decomposition under nonstationary vibration. The PARAFAC decomposition technique is validated using a suite of more than 1400 ground motions and human induced vibration characterized by stationary duration. The effect of lag parameter is studied with respect to the

severity of nonstationarity and the performance of the proposed method is evaluated using fewer number of sensors. Subsequently, the uncertainties associated with the accuracy of the PARAFAC decomposition using optimal sensor locations are also investigated.

2.4   Numerical Simulation

The effectiveness of PARAFAC method depends on the lag parameter and the number of sensors used. In order to investigate the effects of lag parameter (i.e., K) and sensor densities (i.e., n_y) on modal identification, two different building models (5-storey and 10-storey models) and a wide range of earthquakes are considered.

2.4.1   5-DOF model

A 5-DOF system [31] as shown in Fig. 2.4 is used to demonstrate the performance of PARAFAC method under base excitation. The natural frequencies of the model are 0.9, 3.4, 7.1, 10.7 and 12.7 Hz, respectively. Further details of the model parameters can be found in Appendix B. The model underwent a suite of over 1400 ground motions. Resulting vibration responses from the model are processed with the PARAFAC method to extract the modal parameters under a wide range of nonstationary excitation.

Table 2.2 shows six typical ground motions selected as input base excitations in the 5-DOF model along with the detailed information of peak ground acceleration (PGA) and ground motion duration (T). The sampling frequencies of all earthquakes are 50 Hz. The extent of nonstationarity is characterized by the ratio of stationary duration (T_s) [53] and T. T_s [53] may be computed using the time interval containing the energy envelope between 5 and 95 percent of the total energy of an earthquake as shown in Fig. 2.5. An
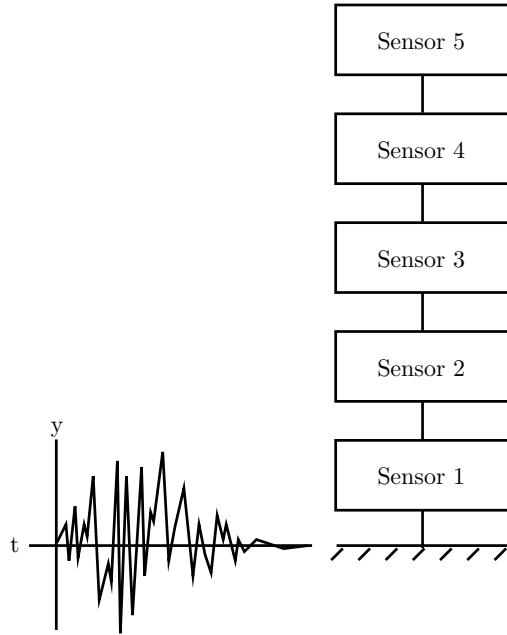
Figure 2.4: Dynamical system subjected to a ground motion

earthquake is considered stationary when the fraction of time between 5 and 95 percent energy is close to 1. On the other hand, when this ratio attains lower value say, ≤ 0.3, the earthquake (i.e., NR and PF) can be considered to be nonstationary. Fig. 2.6 shows the Fourier spectra of the excitation revealing both wideband and narrowband characteristics with respect to the modal frequencies of the model (i.e., $0.9 - 12.7$ Hz). For example, other than EC and KC earthquakes, the energies of the ground motions are distributed in a very narrow frequency range. Furthermore, the example excitation covers a broad range of PGA values with $0.01 - 0.37g$. Therefore, these ground motions form a perfect test-bed to validate the PARAFAC method.

Fig. 2.7 shows the Fourier spectra of top floor measurements of the building under example ground motions. As evident from Fig. 2.6 that most of the energies of the earthquakes are distributed within $0 - 8$ Hz, the first three modes (i.e., 0.91, 3.4 and 7.1
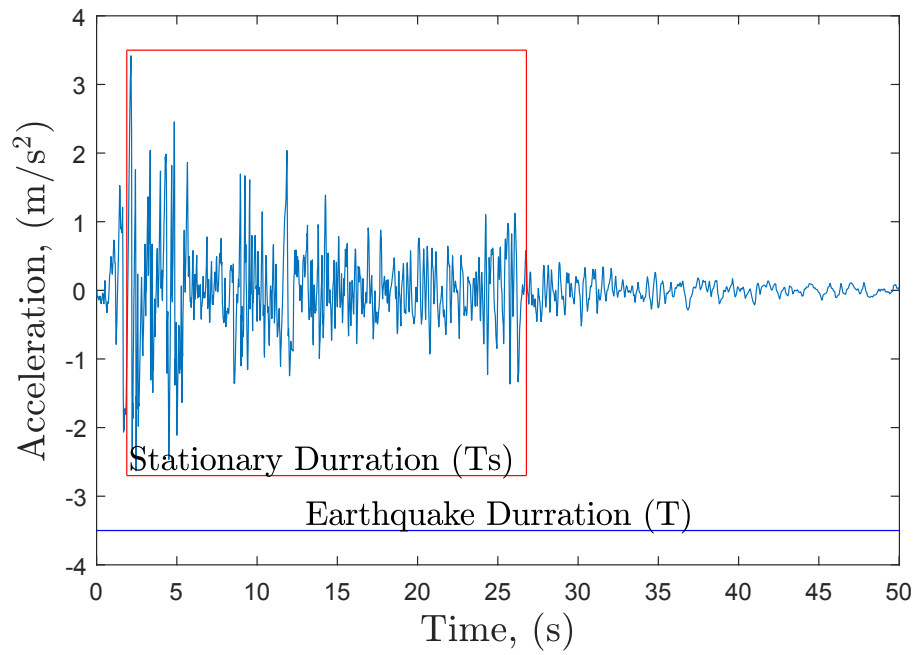
Figure 2.5: Stationary duration of an earthquake

Table 2.2: Details of example ground motions

| Earthquake	PGA (g)	T (s)	$\frac{T_s}{T}$
El Centro (EC), 1940	0.004	50.0	0.50
Northridge (NR), 1994	0.009	60.0	0.12
Imperial Valley (IV), 1940	0.36	53.8	0.47
Kern County (KC), 1952	0.16	54.4	0.63
Parkfield (PF), 1966	0.37	44.0	0.21
San Fernando (SF), 1971	0.02	68.7	0.67

Hz) of the 5-DOF building model fall into this range and are mainly excited as seen in the vibration spectra Fig. 2.7. Therefore, the modal identification of 5-DOF model is restricted to only first three modes.

The response from the typical earthquakes are processed through PARAFAC to present the performance of the proposed method under nonstationary loading. In this section all floor measurements are used with lag of 15 seconds. The resulting Fast Fourier transform (FFT) obtained from PARAFAC are seen in Fig. 2.8, 2.9 and 2.10 for the typical earthquakes. PARAFAC separated out target modes, except for SF. As shown in Fig. 2.10. SF is extremely narrow band with most energy released below 3 Hz leading to its difficultly in exciting higher modes and poor performance.

Effect of Lags

This section will address how the length of lag affects the ability of PARAFAC to separate modal parameters. In order to evaluate the performance of PARAFAC under different lag parameters, lags of 500, 1500, and 3000 (or 2.5, 7.3, and 15 seconds with a sample rate of 200Hz) are undertaken.
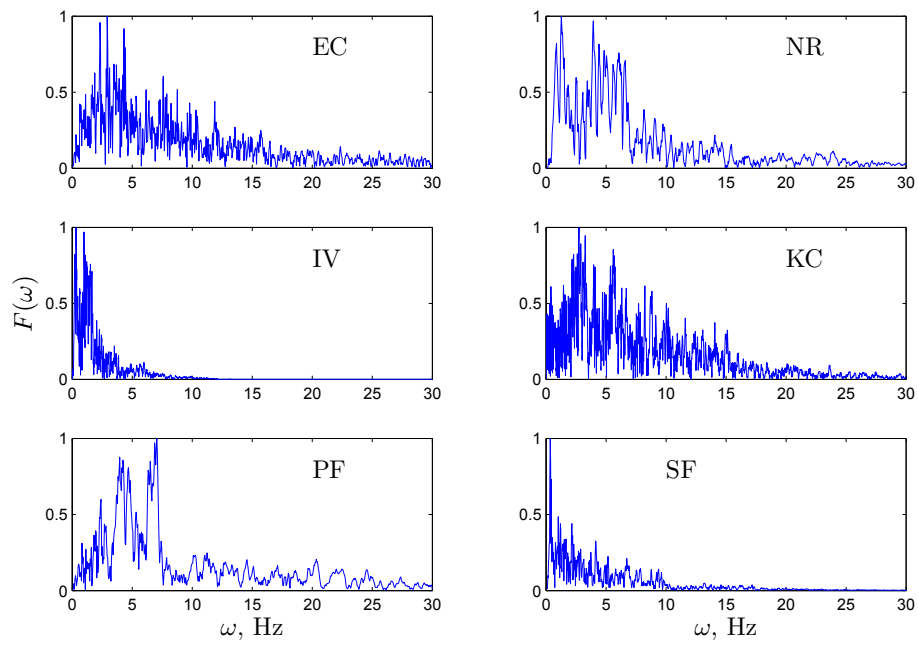
Figure 2.6: Normalized Fourier spectra of example earthquakes
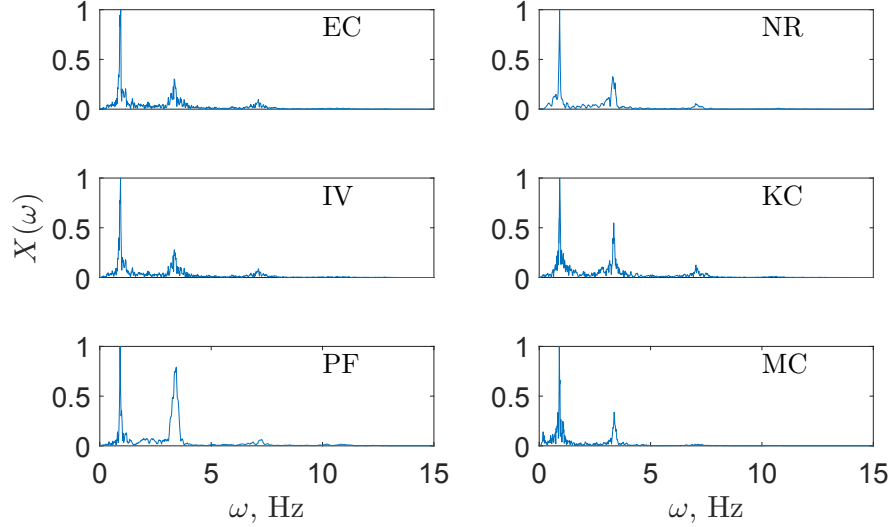
Figure 2.7: Normalized Fourier spectra of top floor response of the 5-DOF model under six example earthquakes

The results from simulations tests reveal the insensitivity towards the choice of lag parameters even under nonstationary vibration. Fig. 2.11 shows the performance of the identified modal parameters using three different lags excited using IV earthquake. Similar results are found for NR and KC earthquakes and the results are shown in Fig. 2.12 and 2.13 respectively. As seen in all three figures PARAFAC is capable of attaining the same modal parameters regardless of the lag chosen. As shown in Table 2.2, NR and KC have extreme $\frac{T_s}{T}$ values ranging between 0.12 to 0.63, even though the PARAFAC method is successful in separating key modal frequencies under any choice of K. Due to tensor representation of covariance matrices under multiple discrete lags and its successive decomposition, the PARAFAC method shows excellent signal separation capabilities in response to nonstationary excitations. Also, it may be noticed that there is sharper resolution associated with a longer lag. It further corroborates its suitability as a possible

25
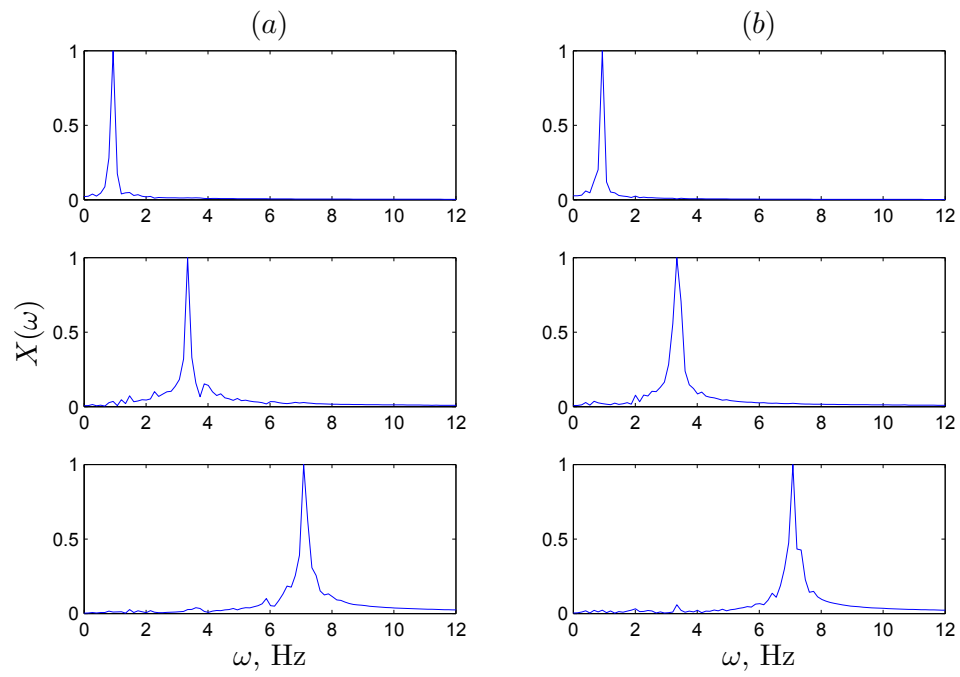
Figure 2.8: Normalized Fourier spectra of identified modal responses under (a) EC and (b) NR earthquake
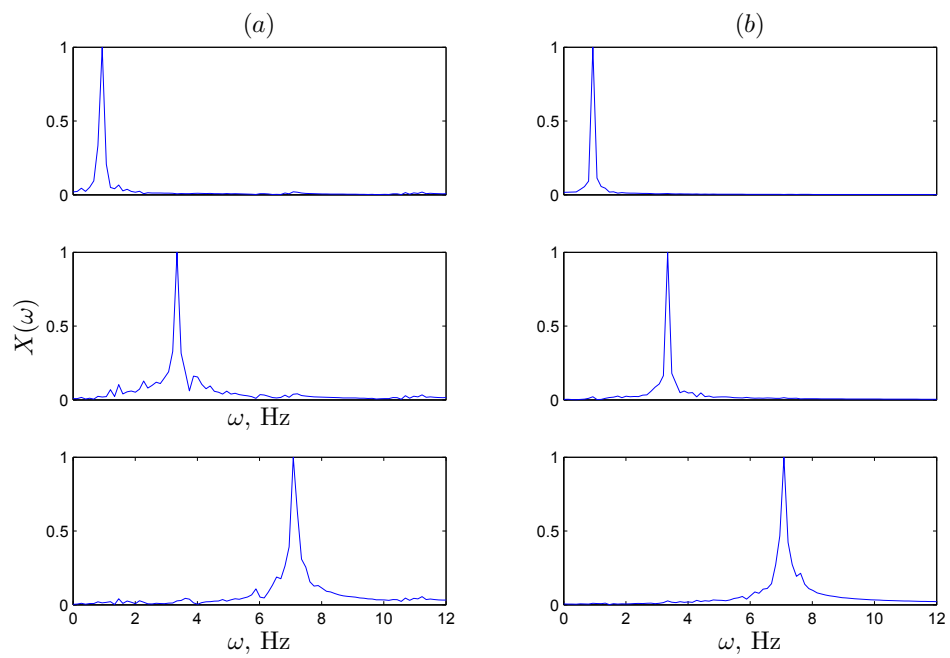
Figure 2.9: Normalized Fourier spectra of identified modal responses under (a) IV and (b) KC earthquake
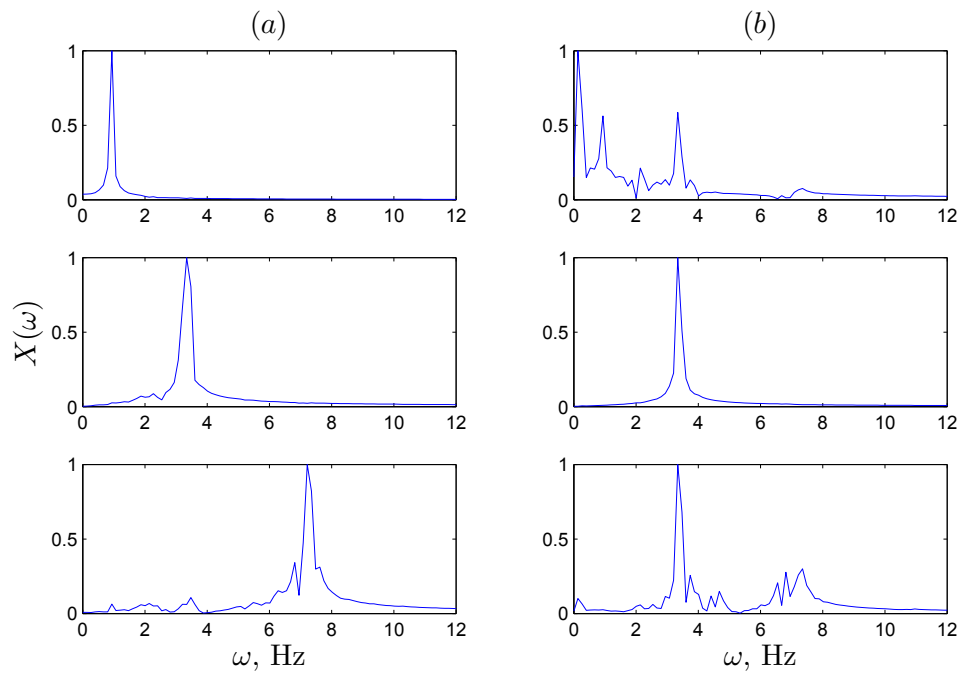
Figure 2.10: Normalized Fourier spectra of identified modal responses under (a) PF and (b) SF earthquake
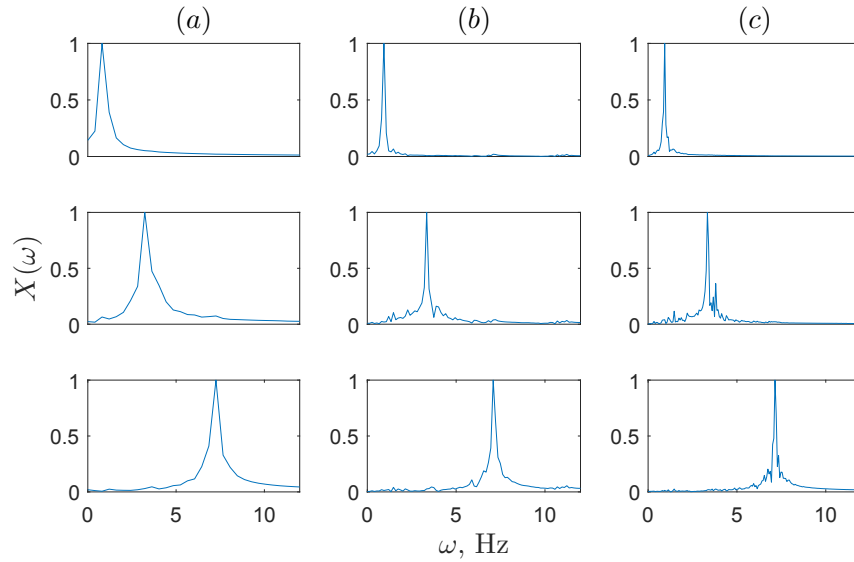
Figure 2.11: Normalized Fourier spectra of identified modal responses under IV earthquake using a lag of (a) 2.5 (b) 7.5 and (c) 15 seconds

modal identification tool to any nonstationary response.

Performance under fewer sensors

A key feature of PARAFAC is its ability to separate signals using a limited number of sensors. Such situations occur due to cost saving, inaccessibility, corrupted data, or malfunctioning of the sensors.

Initial validation removing a number of sensors from a structure is done using the previous 5-DOF model with the six typical earthquakes. Performance of PARAFAC with limited sensors is shown in Fig. 2.14 and 2.15 for NR and KC earthquakes respectively. Results show that removing a sensor does not have a significant impact to the performance of method for low-rise buildings.
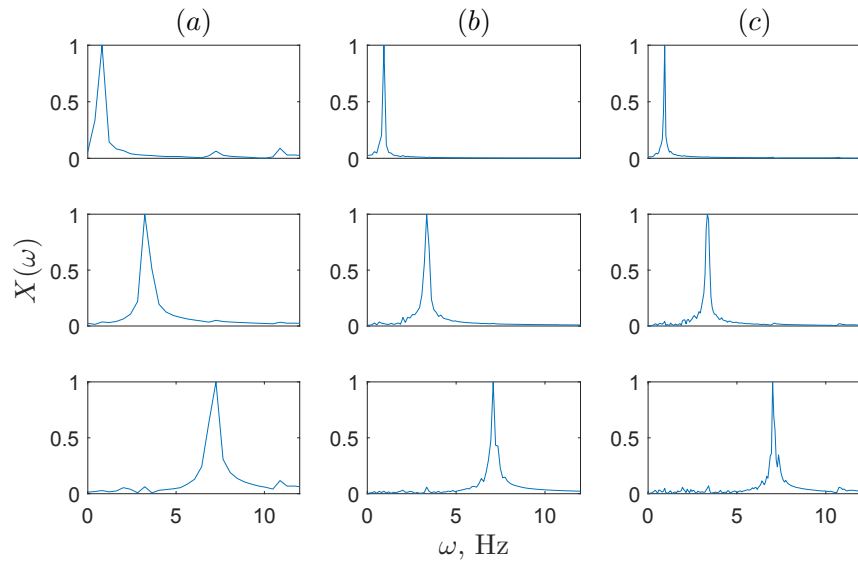
Figure 2.12: Normalized Fourier spectra of identified modal responses under NR earthquake using a lag of (a) 2.5, (b) 7.5 and (c) 15 seconds
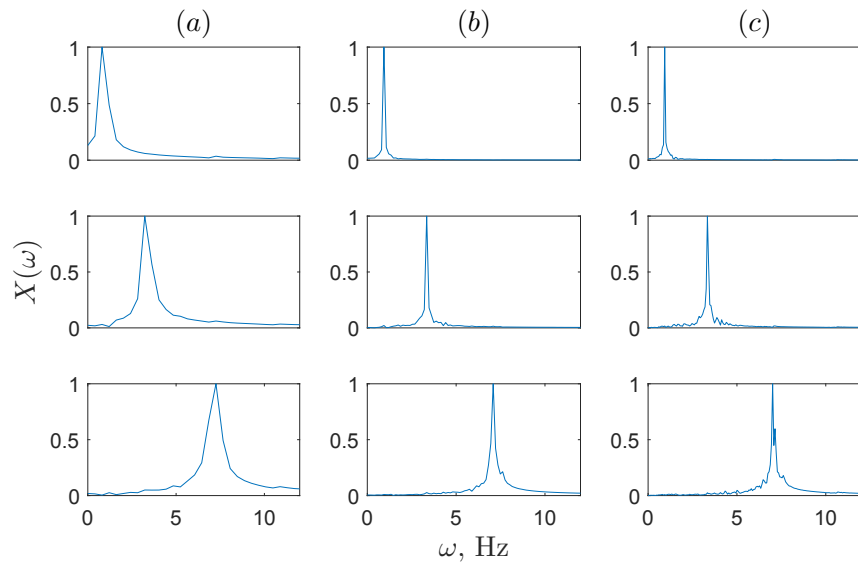
Figure 2.13: Normalized Fourier spectra of identified modal responses under KC earthquake using a lag of (a) 2.5, (b) 7.5 and (c) 15 seconds
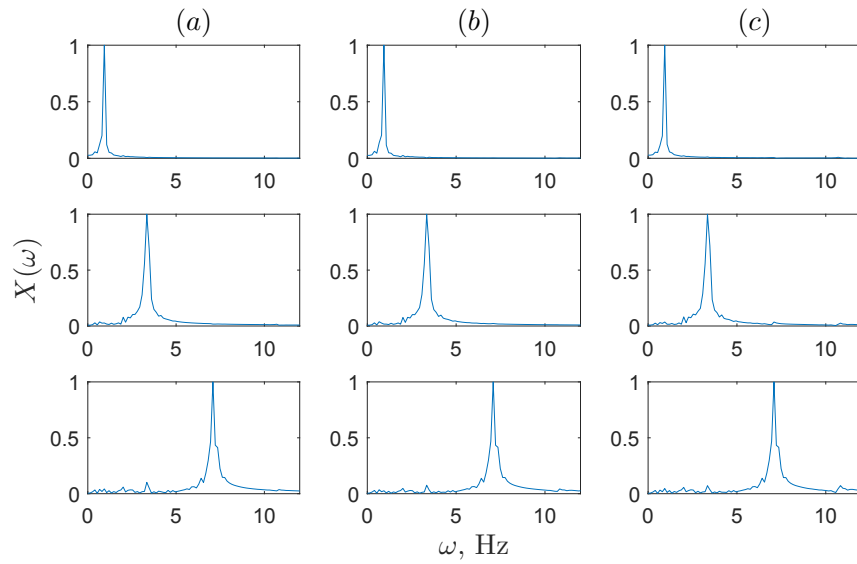
Figure 2.14: Normalized Fourier spectra of identified modal responses under NR earthquake with lag of 2.5 seconds ignoring sensor (a) 2, (b) 4 and (c) 5
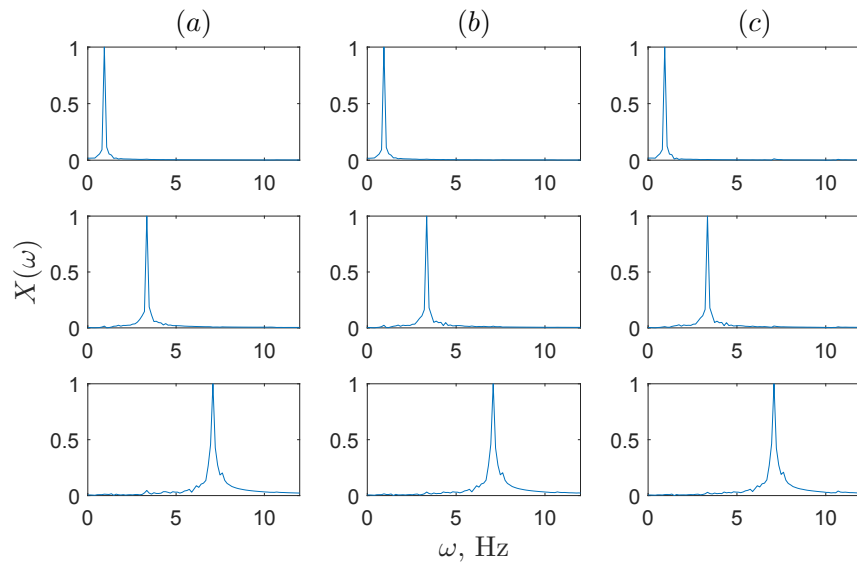
Figure 2.15: Normalized Fourier spectra of identified modal responses under KC earthquake with lag of 2.5 seconds ignoring sensor (a) 2, (b) 4 and (c) 5

A database of 1443 accelerograms is now considered to validate the performance of PARAFAC under a wide range of nonstationarity and sensor combinations. The accelerograms considered in the database were recorded during 14 earthquake events in western U.S.A between 1931 and 1984 [53] and during the 1994 Northridge earthquake. Table 2.4 gives the names of these events along with their magnitudes and the number of records chosen from each event. The 1443 records have been chosen in such a way that the suite has a balanced distribution of records in terms of magnitude, epicentral distance, strong motion duration, and geologic site conditions. All records have PGAs greater than $0.1g$, and have magnitude M ranging from 4.5 to 6.9, epicentral distance R from 4 to 62 km, strong motion duration T_s from 1.8 to 42 s, and site conditions from alluvium to rock.

Table 2.3: Details of the suite of ground motion records used

No.	Event	Magnitude	% of records
1	Imperial Valley, 1940	6.9	8.4
2	Santa Barbara, 1941	5.0	6.2
3	Eureka, 1954	4.5	6.7
4	San Francisco, 1957	5.3	6.2
5	Borrego Mountain, 1968	6.2	5.3
6	San Fernando, 1971	6.6	7.6
7	Oroville, 1975	5.7	6.7
8	Northern California, 1975	5.2	6.2
9	Coyote Lake, 1979	5.9	6.2
10	Imperial Valley, 1979	6.0	9.3
11	Mammoth Lakes, 1980	5.3	5.3
12	Livermore, 1980	5.5	7.6
13	Coalinga, 1983	6.5	4.4
14	Morgan Hill, 1984	6.1	7.1
15	Northridge, 1994	6.7	6.7

Fig. 2.16 and 2.17 show the distribution of PGA and $\frac{T_s}{T}$ ratios of the suite of ground
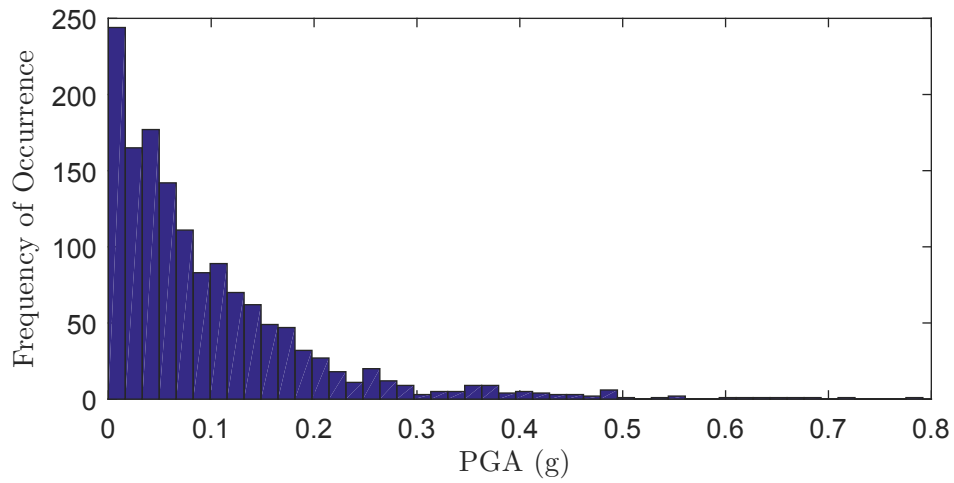
Figure 2.16: Histogram of PGA of ground motion database
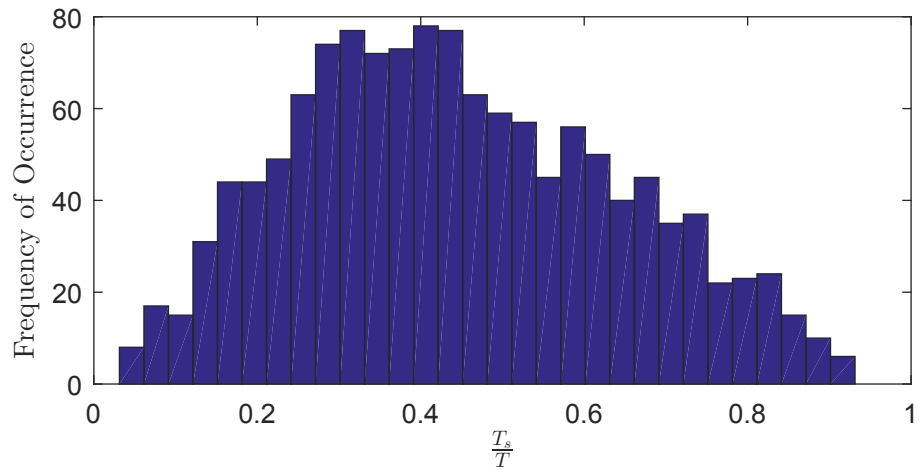
Figure 2.17: Histogram of $\frac{T_s}{T}$ of the ground motion database
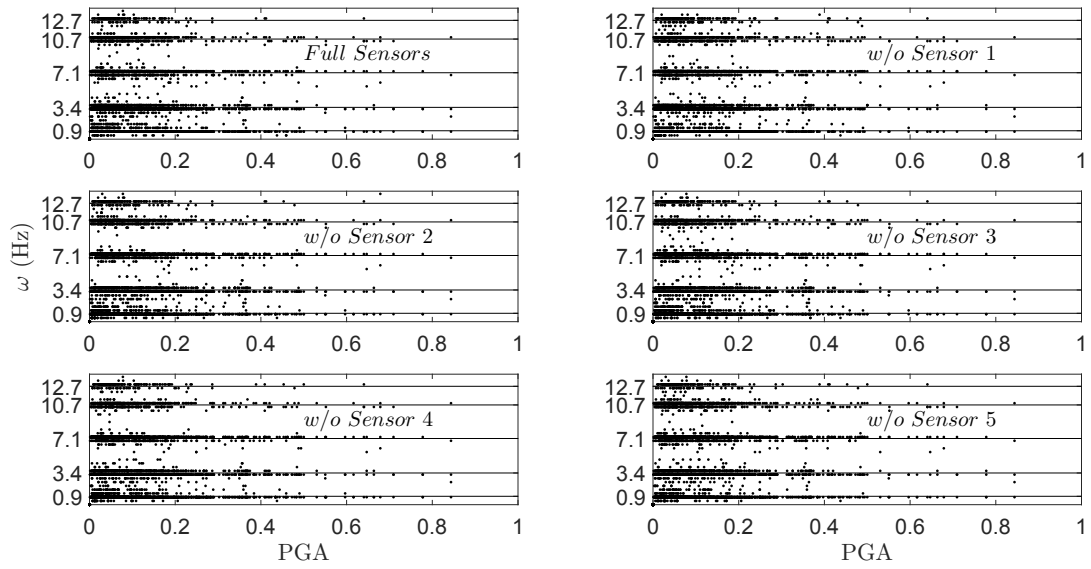
Figure 2.18: Identification results of 5-DOF model w.r.t PGA values under different sensor combinations
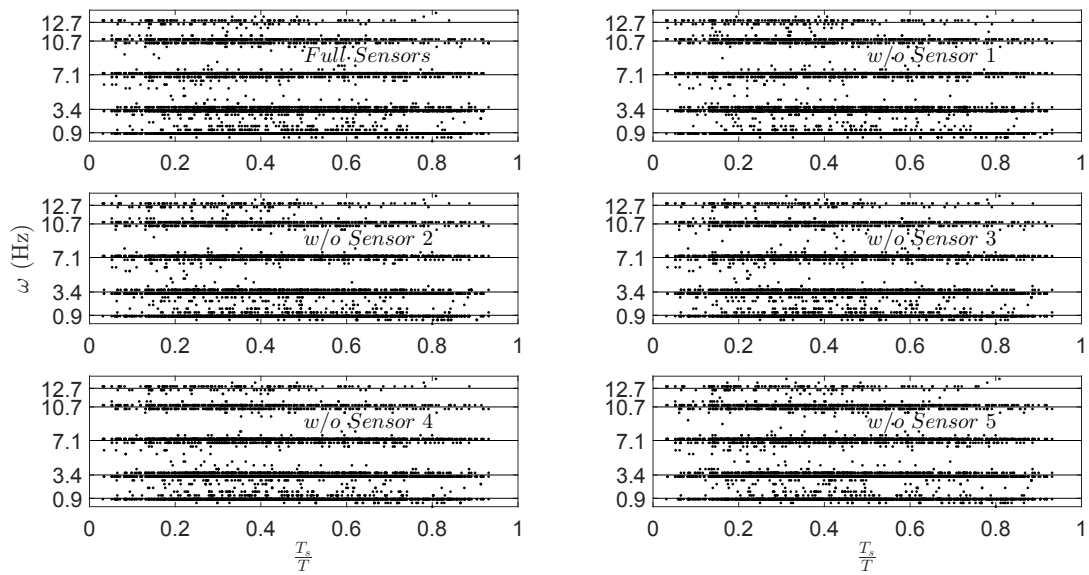
Figure 2.19: Identification results of 5-DOF model w.r.t $\frac{T_s}{T}$ values under different sensor combinations

motions. It reveals that the ground motions form a perfect test bed for the validation purpose with respect to two nonstationary measures (i.e., PGA and $\frac{T_s}{T}$). Fig. 2.18 shows the identification results of the PARAFAC method with the PGA values of earthquake under full sensor (i.e., $n_x = 5$) and fewer sensor (i.e., $n_x = 4$) case using five different sensor combinations (i.e., resulting $C_4^5 = 5$ sensor combinations), while Fig. 2.19 shows similar results w.r.t. $\frac{T_s}{T}$ ratio. In both these figures, solid lines represent exact values of natural frequencies. It is seen that the identified frequencies are nearly clustered with the actual values even under multiple sensor combinations using fewer sensors. These results reveal that the performance of PARAFAC method is insensitive to the location of partial sensors. However it is observed that when $\frac{T_s}{T}$ is more than 0.4 (i.e, with increasing stationarity of earthquake), the clusters of identification results are relatively sparse and associated with less uncertainties. Similar conclusions can be drawn under partial measurement combinations. Therefore, the PARAFAC method can be treated as a robust method under wide range of nonstationary excitations even with complete and partial measurements.

2.4.2   10-DOF model

To further show the effectiveness of limited sensors in the PARAFAC method, a 10 DOF model [56] is now utilized. The natural frequencies of the 10-DOF model are 0.8, 1.8, 2.8, 3.9, 5.0, 6.1, 7.2, 8.5, 9.9 and 11.5 Hz respectively. Using EC, KC, PF and NR earthquakes as the base excitations, the performance of PARAFAC method in 10-DOF model is studied under a wide range of nonstationarities. As shown in Table 2.1, the minimum number of sensors that can be used for a 10-DOF model is 6. Therefore, unlike 5-DOF model (as in section 4.1), 10-DOF model can be effectively used to demonstrate the proposed method under fewer sensors cases owing to their various combinations.
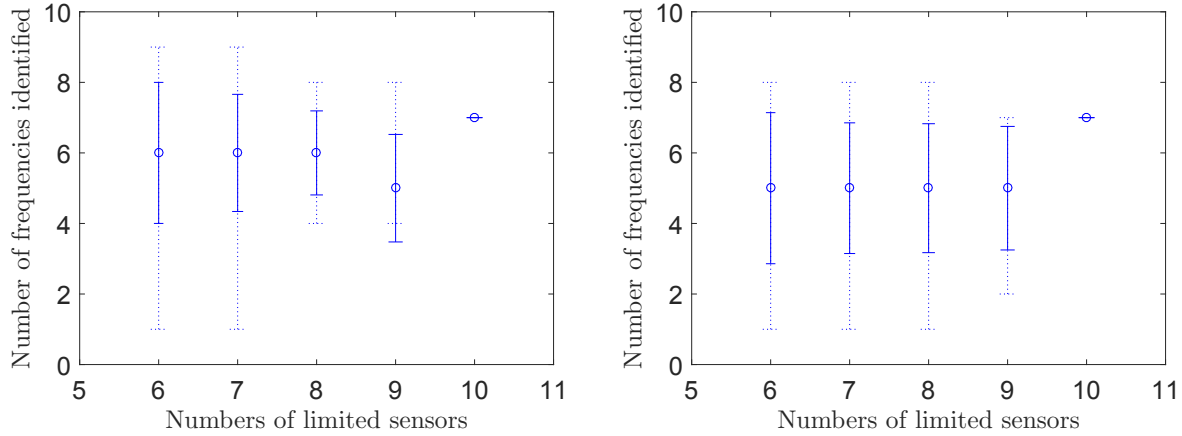
Figure 2.20: Uncertainties in the identification results of 10-DOF model with different sensor configurations for (a) EC and (b) KC earthquake

Table 2.4 shows the number of sensor combinations for the number of limited sensors used. For example, the total number of sensor combinations using 6 sensors is 210. For a specific earthquake and given number of sensors, PARAFAC decomposition is performed for all possible sensor combinations and then the total number of target frequencies are identified. The statistics of the number of identified frequencies are shown in Figs. 2.20 and 2.21 under above mentioned 4 different earthquakes, respectively. The circle represents the average number of frequencies detected. The top and bottom solid lines indicate the standard deviations ($\pm\sigma$), whereas the dotted lines show the range of the number of frequencies identified.

The results reveal that the average number of identified frequencies remains approximately the same irrespective of the number of fewer sensors, however the uncertainties associated with the identification become larger with reduced number of sensor cases. Fig. 2.22 shows the coefficient of variation of the mean number of frequencies of Figs. 2.20 and 2.21 revealing significant accuracy even with fewer number of sensors. With these results,
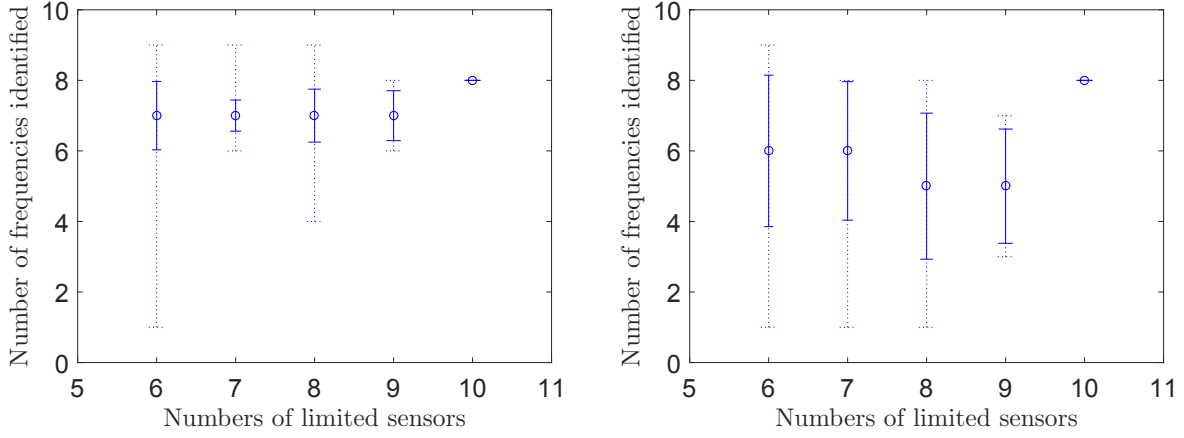
Figure 2.21: Uncertainties in the identification results of the 10-DOF model with different sensor configurations for (a) PF and (b) NR earthquake

it can be concluded that the selection of optimal number of sensors will play a key role to identify the maximum number of target frequencies which however is beyond the scope of present study. Finally, Fig. 2.23 shows the Fourier spectra of identified frequencies using 9 sensors under EC earthquake. The results of the identified frequencies under EC earthquake using 9 sensors are compared with the FE frequencies as well as identified frequencies obtained from the Stochastic subspace identification (SSI) method in Table 2.5. It can be observed that the performance of PARAFAC method is relatively better than the SSI method.

Table 2.4: Number of combinations for different number of limited sensors

No. of sensors	6	7	8	9	10
No. of sensor combinations	210	120	45	10	1
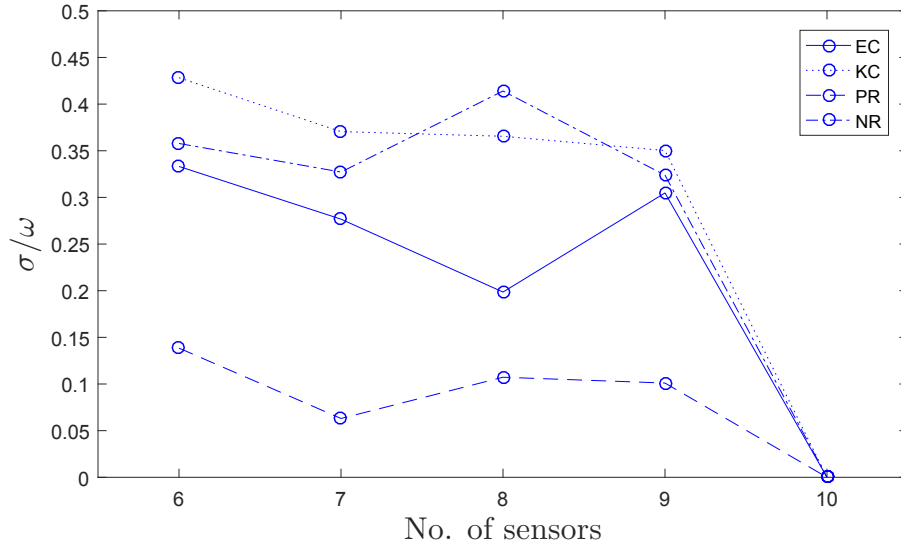
Figure 2.22: Coefficient of variation of identification results under different sensor combinations
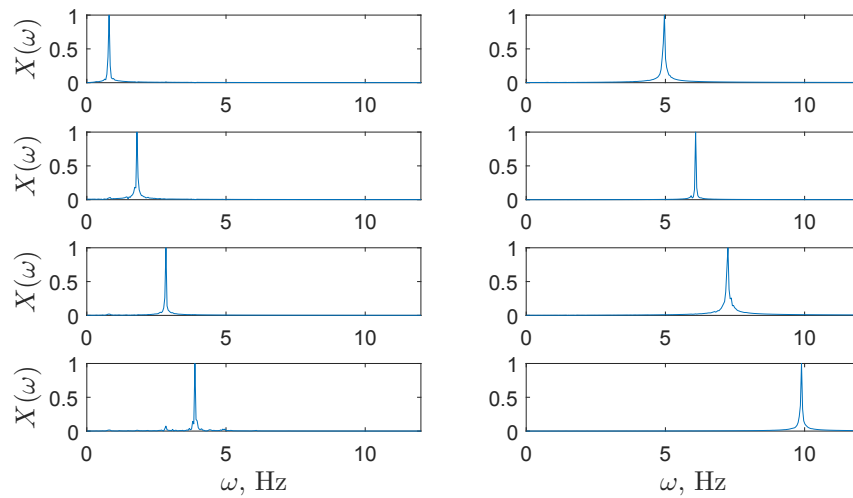
Figure 2.23: Frequencies detected using 9 sensors for EC earthquake (with 1st floor sensor being ignored)

Table 2.5: Identification results of the 10-DOF model under EC earthquake

	ω_1	ω_2	ω_3	ω_4	ω_5	ω_6	ω_7	ω_8	ω_9	ω_{10}
Exact	0.8	1.8	2.8	3.9	5.0	6.1	7.2	8.5	9.9	11.5
PARAFAC	0.8	1.8	2.8	3.8	5.0	6.0	7.3	-	9.9	-
SSI	0.65	1.8	3.2	4.1	5.0	5.5	-	-	8.5	-

2.5 Full-scale Validation

In order to illustrate the proposed method, a footbridge (as shown in Fig. 2.24) crossing the Mcintyre River located in the campus of Lakehead University is utilized under a wide range of pedestrian-induced nonstationary excitations. Designed in 1967, it is composed of two main girders fixed into concrete abutments on both ends with steel struts spaced evenly along the length of the bridge and wooden lumber for decking as shown in Fig. 2.25.

This bridge is instrumented with the accelerometers along the deck to measure the pedestrian-induced vibration. Fig. 2.26(a) shows the layout of the sensor nodes used in this test. A total of eight sensors with a sensitivity of 1V/g are used with 4 distributed evenly on each side of the bridge. The sensors were attached to a data acquisition system operated in a portable computer as shown in Fig. 2.26(b). The sampling frequency was set to 200 Hz. The footbridge was subjected to excitation through a variety of activities such as walking, running, jogging and cycling. The different excitations used during the test are intended to represent the normal operational conditions of the bridge. This bridge mostly sees only light traffic but occasionally is subjected to periods of higher traffic specially during class hours. The excitation tests conducted are described in Table 2.6 including the test duration and T_s/T at the mid span. As listed in the table, T_s/T indicates the extent of nonstationarity present in the vibration data with T_s/T ratio ranging between 0.5-0.8.

Figs. 2.27 and 2.28 show the vibration response of the bridge under single and group

Figure 2.24: Footbridge located in the campus of Lakehead University

Top view

Bottom view

Figure 2.25: Top and bottom view of the bridge
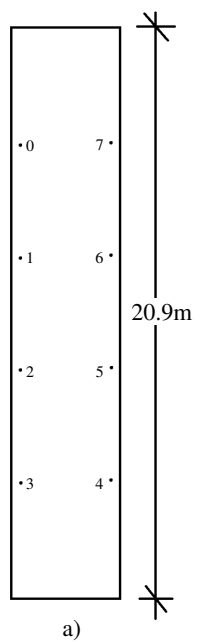
Figure 2.26: (a) Sensor location of the pedestrian bridge, (b) data acquisition system
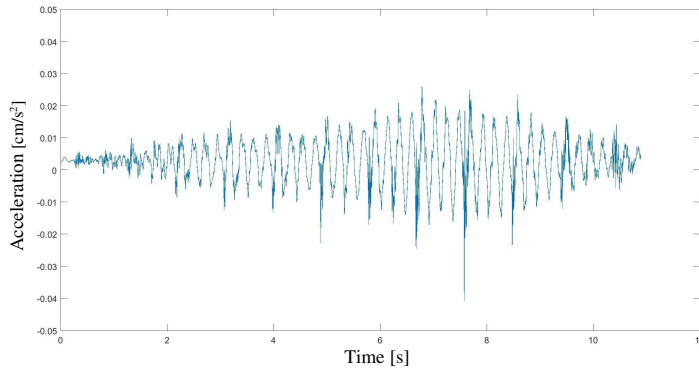
Figure 2.27: Acceleration response of a single person walking

walking as listed in Table 2.6. Due to the nature of transient and spatial excitation over the bridge, it can be seen that the responses are nonstationary which are also reflected through the $\frac{T_s}{T}$ ratio of Table 2.6. For example, sudden jumping is always more nonstatioanry than the gentle walking which is revealed by smaller $\frac{T_S}{T}$ ratio in the jumping data. Therefore, the entire data forms a perfect test bed of the proposed algorithm. In this paper, the vibration data under single running is utilized to validate the performance of the proposed algorithm. The acceleration data is first processed through the PARAFAC method and the resulting modal responses for single run and group walk data are shown in Fig. 2.29. In order to validate the accuracy of the results, a finite element (FE) model of the pedestrian bridge is developed using S-frame software as shown in Fig. 2.30. The identified frequencies (4.2, 11.8 and 28.5 Hz) are reasonably matching with the FE frequencies. Slight discrepancies may be observed due to inexact modeling and lack of structural details of the pedestrian bridge.
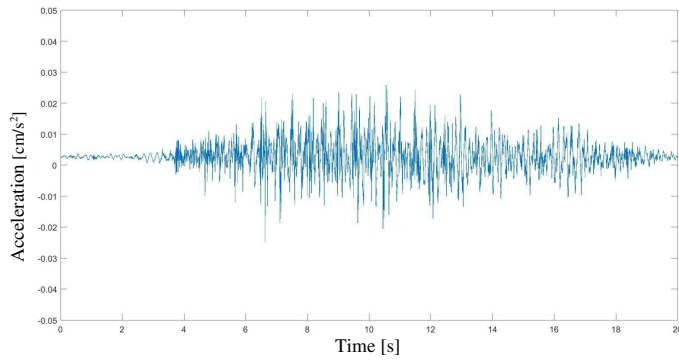
Figure 2.28: Acceleration response of group walking
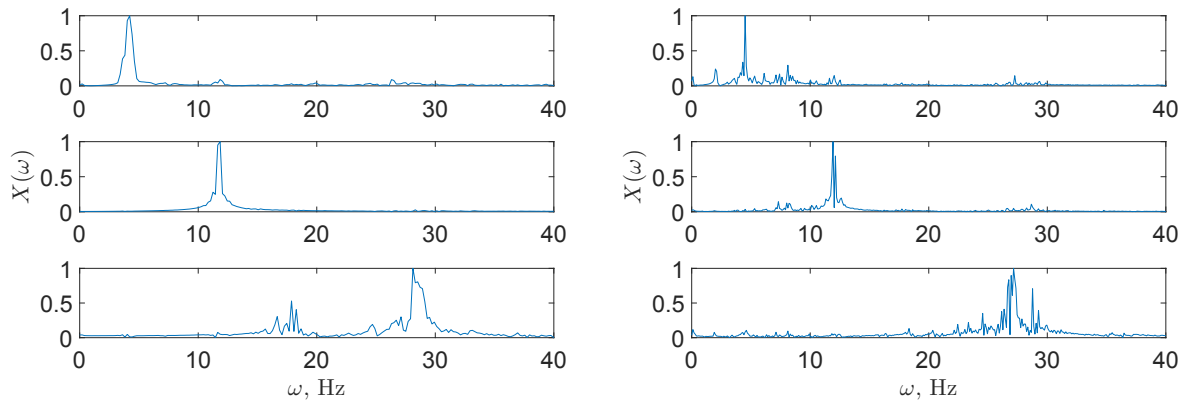
Figure 2.29: Normalized Fourier spectra of identified modal responses under (a) single running test and (b) group walking test

a)   b)   2.7 Hz

c)   11.7 Hz   d)   30.8 Hz
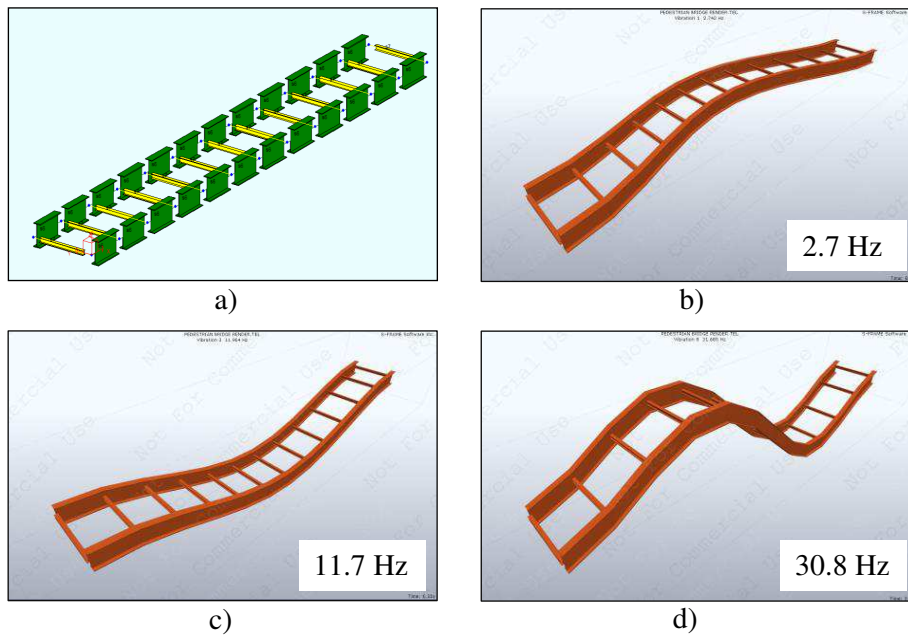
Figure 2.30: FE model and its modeshapes

Table 2.6: Details of vibration testing in the footbridge

Test	Details	T (s)	$\frac{T_s}{T}$
Single walking	A single person walked at a normal pace across the bridge	10.9	0.62
Group walking	A group of four people walked at a normal pace across the bridge	20.1	0.61
Single running	A single person ran at a jogging pace across the bridge	7.2	0.53
Group running	A group of four people ran at a jogging pace across the bridge	12.9	0.54
Single jumping	A single person jumped at the center of the bridge	12.5	0.52
Group jumping	A group of four people jumped at the center of the bridge	7.7	0.6
Biking	A single person rode a bicycle at a normal pace over the bridge	10.1	0.79

Chapter 3

Proposed Method

In this chapter, tensor decomposition is integrated with continuous wavelet transform to undertake modal identification of time-varying systems or progressively damaged structure. The proposed method is validated using several numerical models and an experimental model where time-varying characteristic is simulated using a heating torch.

3.1 Introduction

As discussed in section-1.3, there has been a limited amount of research related to the topic of progressive structural damage. This work seeks to develop a method capable of separating structural modes and tracking progressive changes in modal parameters over time. With the improved performance of PARAFAC decomposition under amplitude-dependent nonstationary response, an attempt is made to identify frequency-dependent nonstationarity next. In this chapter, PARAFAC decomposition is integrated with Cauchy continuous wavelet transform (CCWT), a special type of Continuous wavelet transform

(CWT). PARAFAC is first used to separate the signals into modal responses which are tracked in the time-frequency domain with CCWT.

3.2 Background

The Fourier transform (FT) is one of the classical tools for determining the frequency content of a time-invariant system. A major shortcoming of Fourier transform is the lack of its time information that is essential to detect progressive damage or time-varying system. Unlike FT, short-time Fourier transform (STFT) decomposes a signal into smaller windows and performs frequency domain analysis in each time window. The WT is primarily categorized into two different classes: discrete and continuous wavelet transforms. With appropriate basis function, the wavelet transform (WT) offers excellent flexibility to achieve better time and frequency resolutions together.

The CWT is a highly adaptable [5, 4] signal processing technique that is used for many applications such as signal noise filtering, image compression, and medical signal processing. The CWT is used to separate mixed signals into their components as well as filtering out noise and it is given by:

$$W_f(s, \tau) = \int_{-\infty}^{\infty} f(t) \frac{1}{\sqrt{s}} \psi^* \left(\frac{t - \tau}{s} \right) dt \tag{3.1}$$

The inverse continuous wavelet transform is defined as,

$$f(t) = \frac{1}{C_\phi} \int_0^\infty \int_{-\infty}^{\infty} W_f(s, \tau) \frac{1}{\sqrt{s}} \psi \left(\frac{t - \tau}{s} \right) d\tau \frac{ds}{s^2}, \tag{3.2}$$

Where C_ϕ is defined as

$$C_\phi = \int_0^\infty \frac{|\Phi(\omega)|^2}{\omega} d\omega < \infty \tag{3.3}$$

Where, s and τ represent scale and translation of the mother wavelet, respectively. s relates to frequency scale, where a larger value of s relates to low frequency signal and smaller s relates to a high frequency signal. At a location where the signal's spectral component is similar in scale to the value s, the product between the wavelet and signal will be higher. The wavelet shifts along the signal to locate the frequencies within the time domain. The basis function is called mother wavelet $\psi(t)$. The superscript denotes its complex conjugate. With the appropriate choice of a and b, the CWT utilizes the shifted and scaled versions of ψ and subsequently forms its inner product with $f(t)$.

Le and Argoul [30] implemented CWT for system identification of linear multi-DOF systems and tested the performance of different mother wavelets. The work found that the Morlet and Cauchy mother wavelet can be employed to extract frequencies, modal damping and modeshapes from a free vibration response. The Cauchy CWT (CCWT) has the benefit of its ability to processes acceleration, velocity or displacement data. In another study, CCWT was further used to identify the damping ratios and modeshapes from the free response of linear systems with non-proportional damping [18]. This work also addressed the selection of optimal Q-factor to reduce errors in the damping estimation. Argoul and Le [8] used the CCWT to detect non-linearity in the beam under an impact force. Recently, the CCWT has been further used with autoregressive methods to determine the location of damage in nonlinear systems [29, 50] and time variant systems [22]. They showed that the CCWT can be a valuable tool for SHM.

In this paper, the CCWT is explored as a method to detect time-varying progressive damage in structural systems owing to its strong detection capability under frequency-modulated signals [39]. Fig. 3.1 shows the Cauchy mother wavelet where the single peak is well suited to signals with non-stationarity in frequency. Fig. 3.2 shows the CCWT of a sine signal that undergoes an instantaneous change in frequency from 8 to 10 Hz.
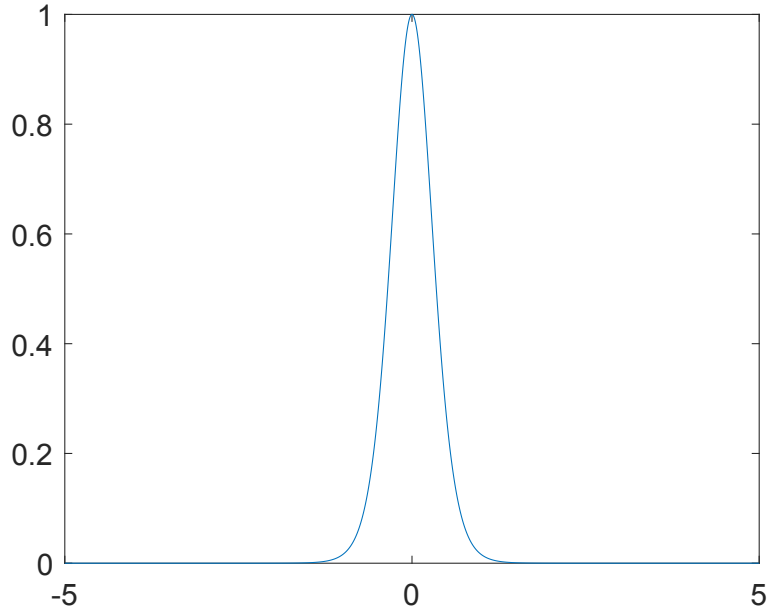
Figure 3.1: Cauchy mother wavelet

Fig. 3.3 shows the CCWT of a sine sweep signal where the frequency is changing between 3.0 and 8.0 Hz with 20% noise contamination. The results show that the CCWT tracks the signal quite well with the exception of distortion in boundary that cause end-effects similar to previous studies [14]. It is also seen how the CCWT provides better resolution for lower frequencies. These abilities makes it well suited for identifying progressive damage in structural systems with low frequencies.
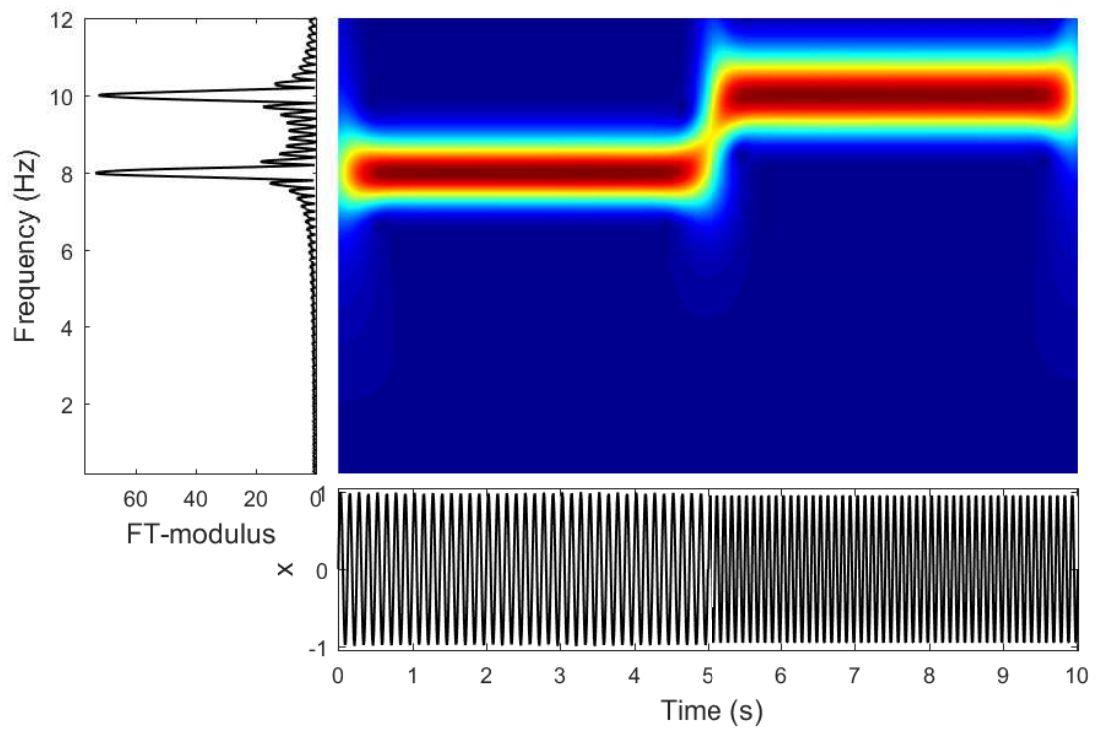
Figure 3.2: The CCWT of sine signal where the frequency is discretely changed from 8 to 10 Hz
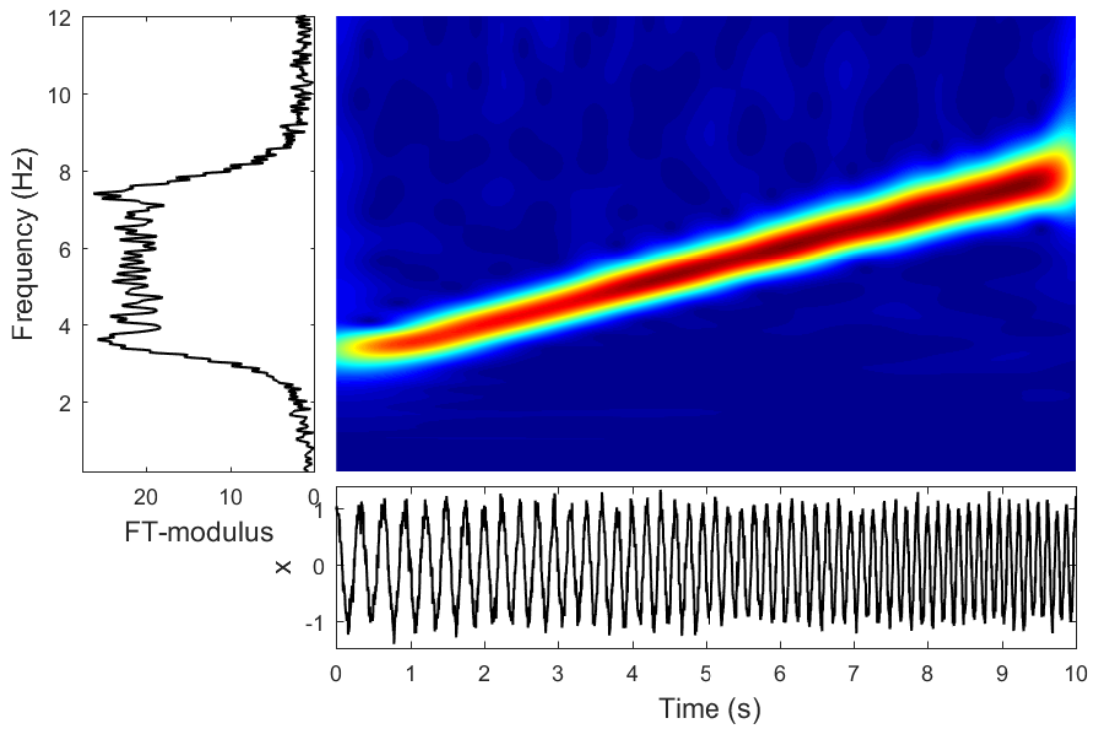
Figure 3.3: The CCWT of sine sweep signal having variation in frequency from 3 to 8 Hz with 20% noise

3.3 Formulation

In previous chapter, it is verified that the PARAFAC-based tensor decomposition method is suitable to undertake modal identification under amplitude-dependent nonstationary excitation caused by the natural hazard. However when there is a damage in structure, it further introduces frequency-dependent nonstationary in the response due to *progressive* time-varying nature of natural frequencies of the structures. With unique time-varying characteristics and subsequent frequency resolution of the CCWT, the CCWT is now integrated with the PARAFAC decomposition to perform modal identification using both amplitude and frequency-dependent nonstationary response.

In CCWT, $\psi(t)$ is defined as follows [8]:

$$\psi\left(t\right) = \psi_{\beta,n}\left(t\right) = \left(\frac{i}{\beta t + i}\right)^{n+1} \tag{3.4}$$

where, n is a non-dimensional positive parameter ($n > 1$) and adjusts the frequency resolution of the signal. β is a positive parameter whose dimension is the inverse of the dimension of the variable t. Fourier transform of $\psi(t)$ is derived as [8]:

$$\hat{\psi}\left(\omega\right) = \hat{\psi}_{\beta,n}\left(\omega\right) = 2\pi \left(\frac{\omega}{\beta}\right)^n \frac{e^{-\frac{\omega}{\beta}}}{n!} H\left(\omega\right) \tag{3.5}$$

where $H(\cdot)$ is the Heaviside step function. Due to the choice of the Heaviside function, the CCWT has time-varying properties where its Fourier transform vanishes rapidly. This property is utilized here to track the progressive change in the natural frequencies of structures. The CCWT is then utilized over the PARAFAC components to track the frequency changes over time.

As derived in Eq. (3.6), for any general n_d-DOF dynamical system, the tensor decomposition of the covariance tensor of vibration measurements yield,

$$Z_{ijk}^{y} = \sum_{r=1}^{n_d} \Gamma_{ir}\Gamma_{jr}Z_{kr}^{q} \iff \mathbf{Z^y} = \sum_{r=1}^{n_d} \mathbf{\Gamma_r} \circ \mathbf{\Gamma_r} \circ \mathbf{Z_r^q}. \tag{3.6}$$

where $\mathbf{Z_r^q}$ represents the r-th modal responses of the structure. With progressive damage, it is anticipated that the natural frequency of each modal responses will be time-varying in nature. Therefore, the CCWT is applied to each $\mathbf{Z_r^q}$ separately to track the changes in the frequencies. Using Eq. (3.1), the CCWT of $\mathbf{Z_r^q}$ can be obtained as,

$$W_f^{Z}(s,\tau) = \int_{-\infty}^{\infty} Z_r^{q}(t)\frac{1}{\sqrt{s}}\psi^*\left(\frac{t-\tau}{s}\right) dt \tag{3.7}$$

where ψ is given by Eq. (3.4) and the superscript denotes its complex conjugate.

Chapter 4

Results and Discussions

In this section, the proposed method is validated through a wide range of numerical simulations and experimental studies. In order to illustrate the application of the CCWT in a dynamical system, the CCWT is directly applied in a SDOF system first. The proposed method is then illustrated using two simulation models: (a) 2-DOF model and (b) 4-DOF model. Finally, an experimental model is used to identify progressive damage using the proposed method.

4.1   SDOF Model

A single DOF system is first selected to test the performance of the CCWT. A 10 kg model with a progressive stiffness reduction from 5000 to 1000 N/m between 20-30 seconds is used for the illustration. The model has undamaged and damaged natural frequency of 3.6 Hz and 1.6 Hz, respectively. The performance of the CCWT using the vibration response of the SDOF model subjected to a harmonic frequency of 2.6 Hz and 5 Hz are shown in Fig.
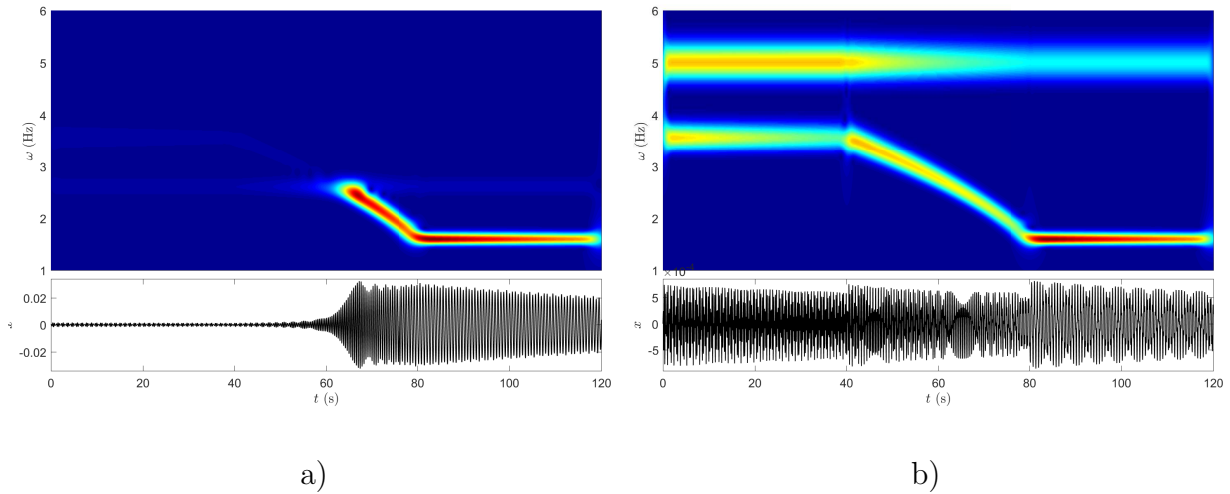
Figure 4.1: The CCWT of the response of SDOF system subjected to harmonic excitation with a frequency of (a) 2.6 Hz and (b) 5 Hz

4.1, respectively. In Fig. 4.1(a) an increase in amplitude can be seen since the system's natural frequency matches with the forcing frequency (i.e., 2.6 Hz) at 65 seconds. Whereas Fig. 4.1(b) shows a separate frequency of 5 Hz along with accurately tracking of progressive changes of natural frequencies. Therefore, the CCWT provides a better picture of what is happening to the system than any other frequency or time-domain methods.

In order to test the performance of the CCWT under nonstationary vibrations, the SDOF is excited using El Centro earthquake. Validation is conducted using both displacement and acceleration data. As shown in Fig. 4.2(a), the CCWT of the displacement data clearly shows the change in frequency. Fig. 4.2(b) shows the CCWT of the acceleration data. The changes in frequency are visible, however it is harder to follow after 30 seconds due to low amplitude. Bot h figures show the progressive damage that starts at 20 seconds and ends near 30 seconds, thereby they correctly match with actual damage instants.

56
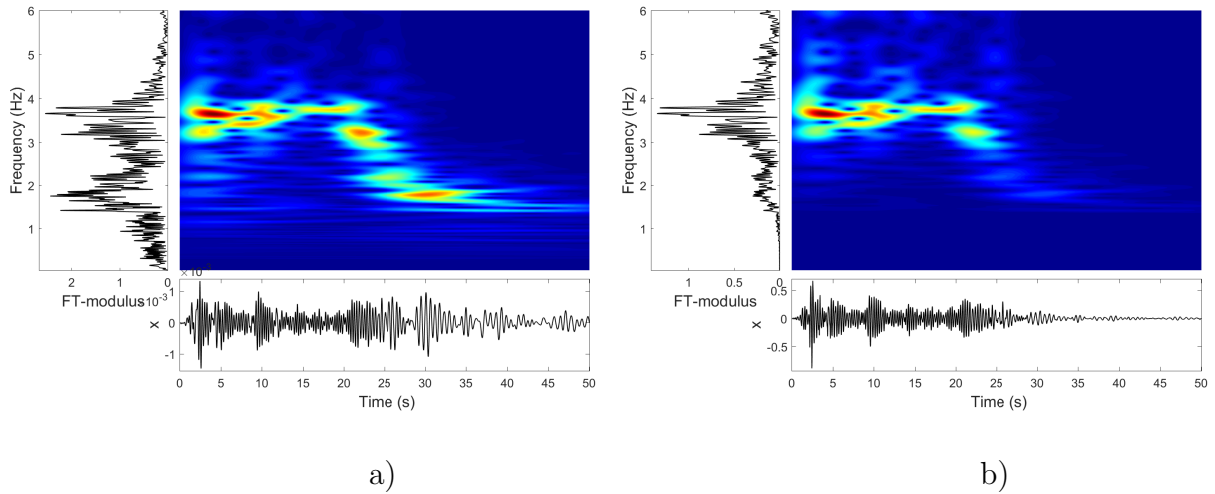
Figure 4.2: The CCWT of the response of SDOF system subject to El Centro earthquake using (a) displacement and (b) acceleration data

4.2   2-DOF Model

As shown in Fig. 4.3, a 2-DOF simulated model is developed to validate the proposed method. The model has natural frequencies as 1.9 and 3.9 Hz, respectively where the damage is simulated with a linear stiffness degradation introduced at 10th seconds and continued till 30th seconds. The resulting acceleration response of the model subjected to El Centro earthquake is shown in Fig. 4.4. Fig. 4.4(b) shows the Fourier spectrum of the floor responses, respectively. The PARAFAC is first implemented over the responses and the resulting Fourier spectra of the separated sources are shown in Fig. 4.5. The figure shows that the PARAFAC clearly separated both its modal responses.

The CCWT is then applied on the separated sources and tracked the frequency of the modal responses over time. The results are shown in Fig. 4.6 that confirms the change in frequency due to damage between 10 and 30 seconds. Therefore, the algorithm is able to
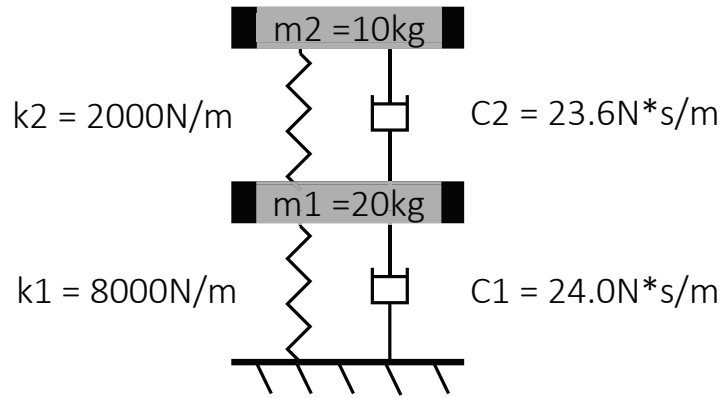
Figure 4.3: 2-DOF Model

a)

b)
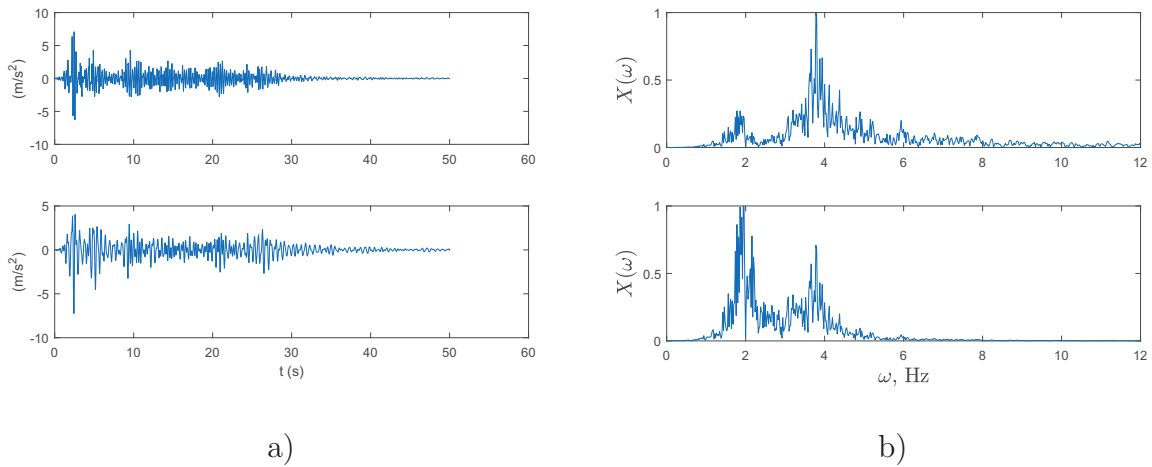
Figure 4.4: System response of the 2-DOF model under El Centro earthquake and the corresponding Fourier spectra of the response

58
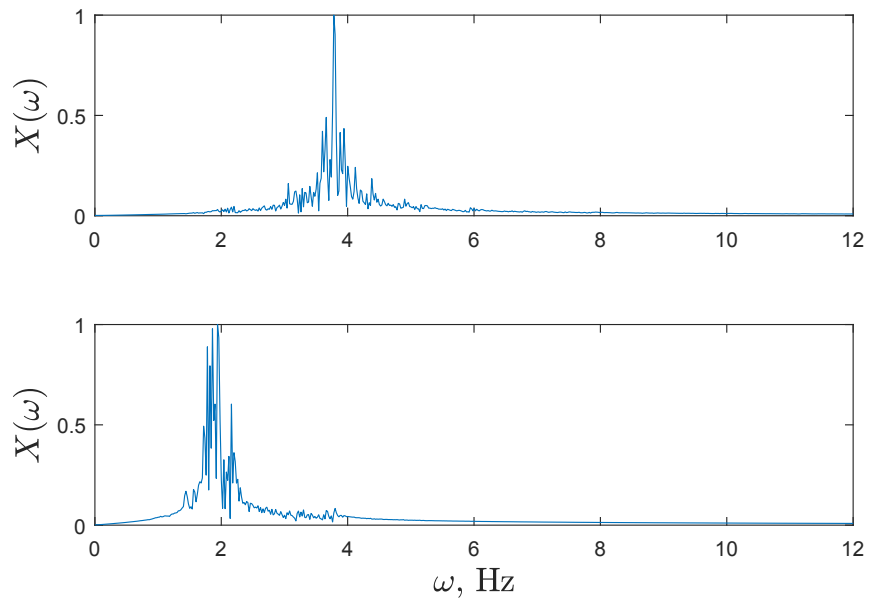
Figure 4.5: Fourier spectra of the separated modal responses using the CCWT

a)   b)
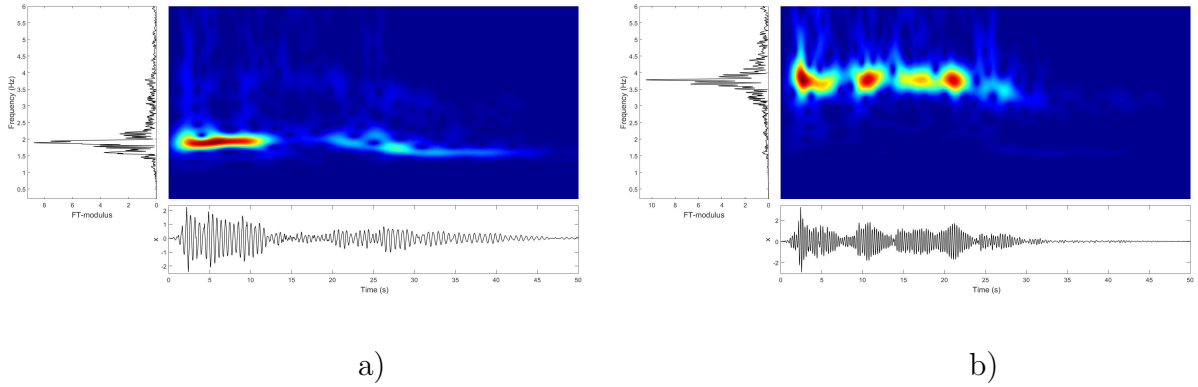
Figure 4.6: The CCWT of the (a) 1st and (b) 2nd modal responses

separate and track the change in frequency.

4.3   4-DOF Model

In this section, a 4-DOF modal is used as shown in Fig. 4.7. Various different damage scenarios are conducted as listed in Table 4.1 to check the sensitivity and accuracy of the proposed method. For example, Case 1 represents 50% damage in the first floor and no other damages in the subsequent floors. All the damages are simulated through a linearly stiffness reduction between 50th and 80th seconds. The frequencies for the undamaged and damage cases are shown in Table 4.2

Fig. 4.8 shows the floor vibration data and the corresponding Fourier spectra of the data under Case 1. Fig. 4.9 shows clear separation of all four modes of the 4-DOF model once PARAFAC is applied on the vibration response. The results of CCWT for Case 1 are shown in Fig. 4.10. There is a clear frequency shift in the first (a) and second (b) modes, respectively. For example, the first mode has a frequency change from 0.68 to 0.60 Hz between 58 and 80 seconds. For the higher modes, the changes in frequencies are very

60
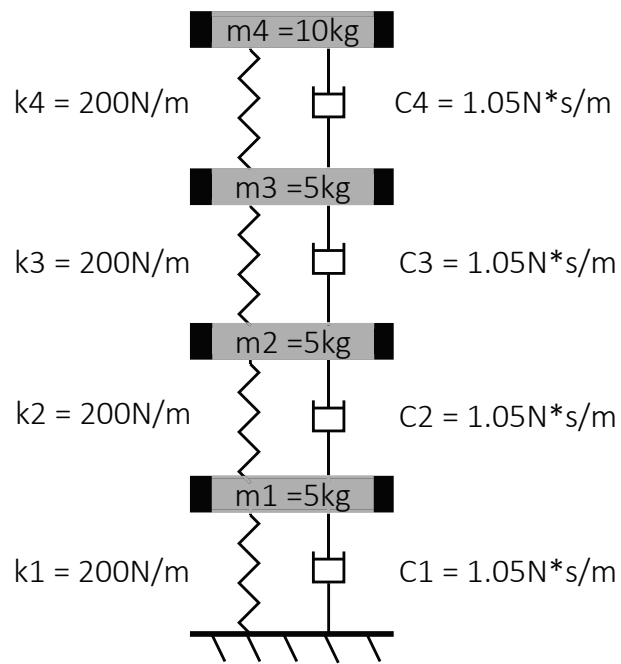
Figure 4.7: 4-DOF Model

Table 4.1: Damage scenarios

Cases	1st Floor	2nd Floor	3rd Floor	4th Floor
1	50%	0	0	0
2	50%	40%	0	0
3	50%	40%	30%	0
4	30%	30%	30%	30%

minor which are not reflected in the data.

As the damage increases for cases 2, 3, and 4, the frequency separation becomes wider and more distinct. Figs. 4.11, 4.12, and 4.13 show the CCWT of damage cases 2, 3, and 4, respectively. The results for the Case 4 as shown in Fig. 4.13 clearly identify the progressive damage in all four modes.

4.4   Experimental Validation

4.4.1   Experimental Setup

In order to validate the proposed method, an experimental model as shown in Fig. 4.14 is developed where progressive damage is artificially simulated in the bracing through a heating torch. The structure is comprised of four aluminium columns with a width of 25.5 mm and thickness of 1.5 mm. The floors are made of steel rectangular plates. The lower
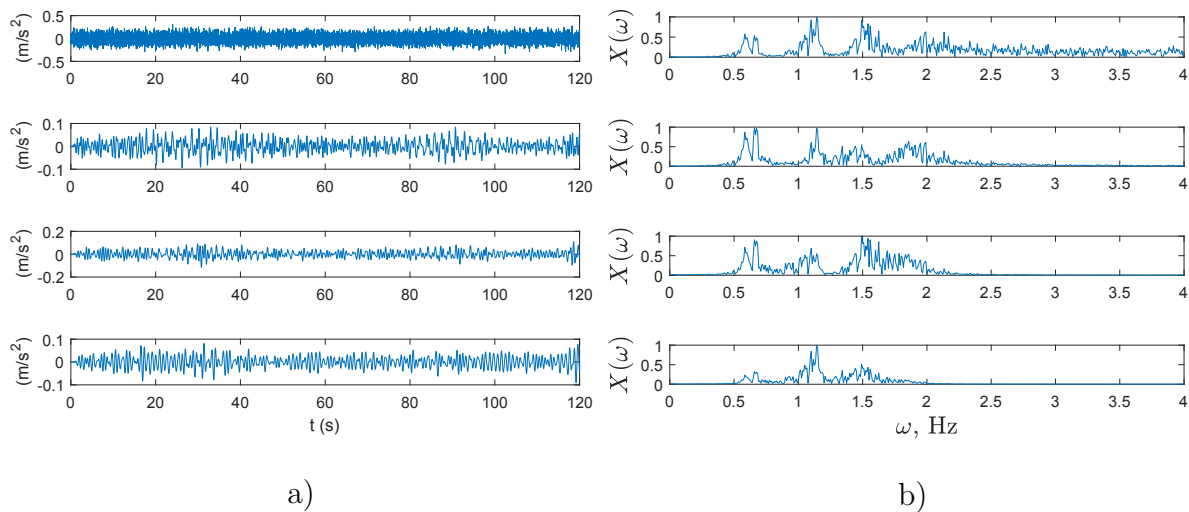
Figure 4.8: Case 1: (a) response data and b) Fourier spectra
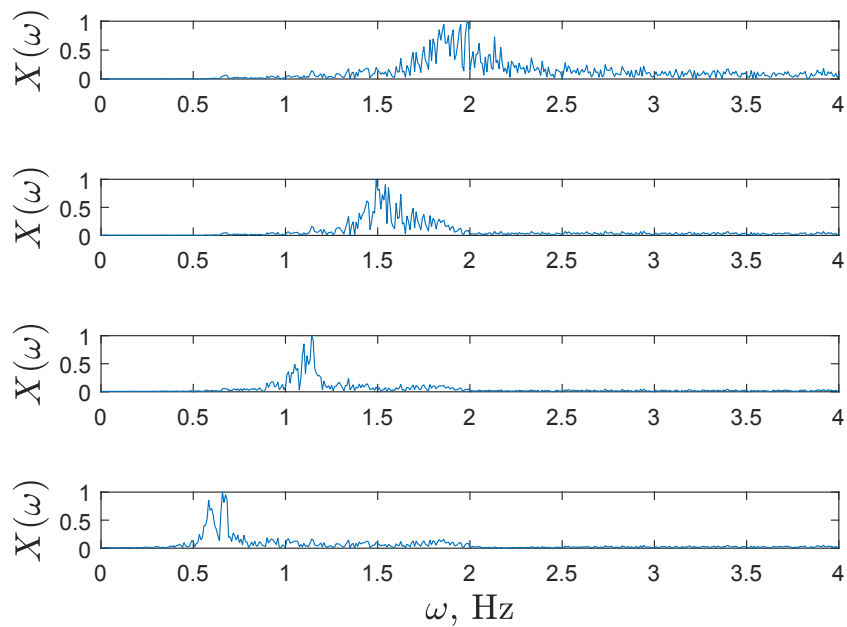
Figure 4.9: Fourier Spectra of separated modal responses under Case 1

63
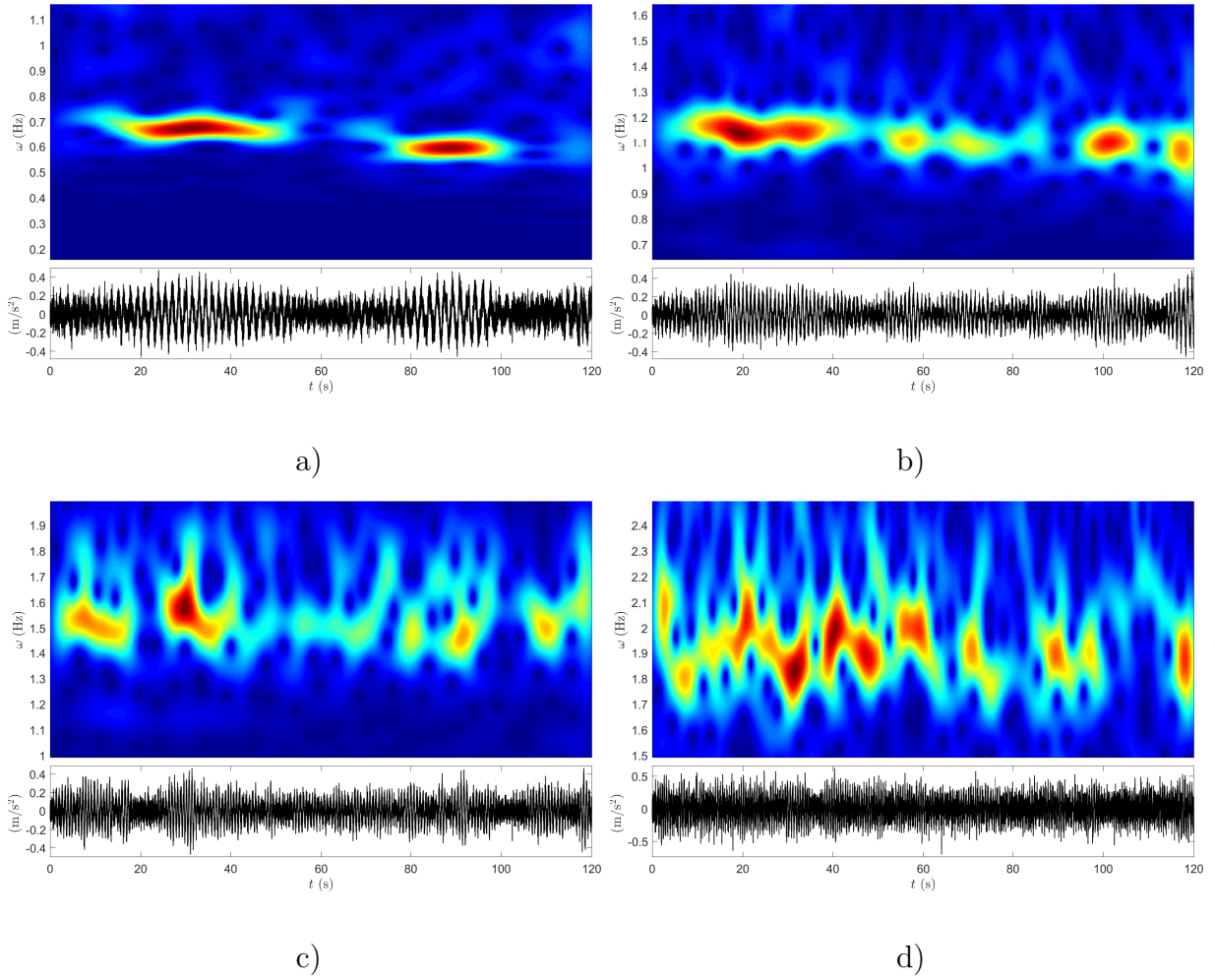
Figure 4.10: The CCWT of (a) 1st, (b) 2nd, (c) 3rd, and (d) 4th modes under Case 1
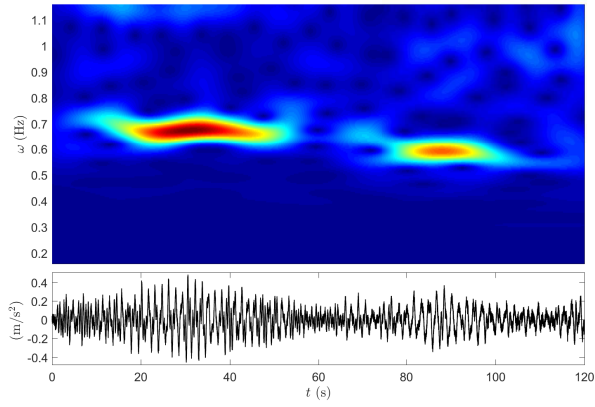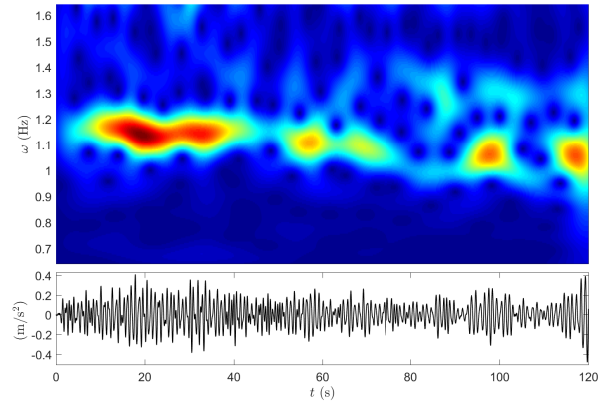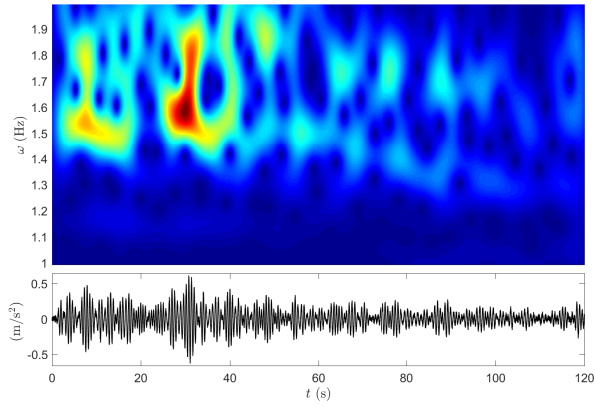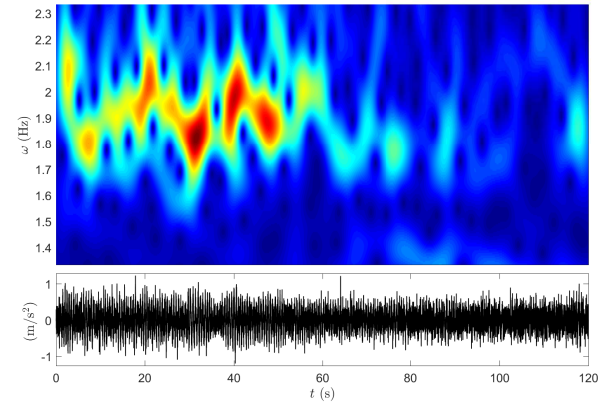
Figure 4.11: The CCWT of (a) 1st, (b) 2nd, (c) 3rd, and (d) 4th modes under Case 2
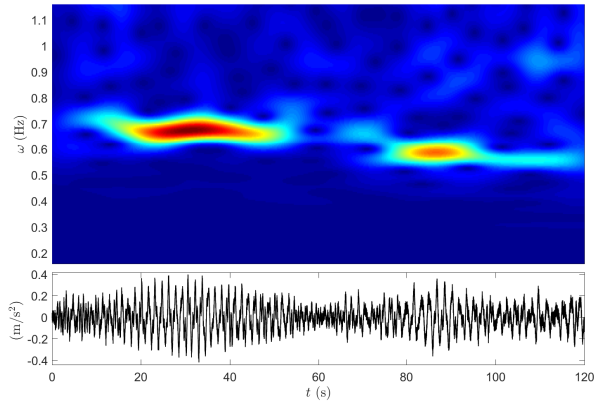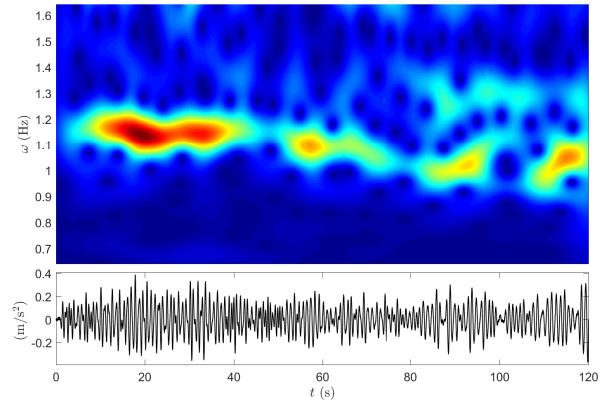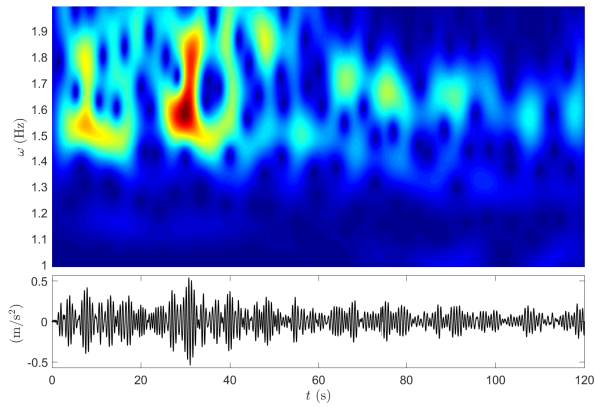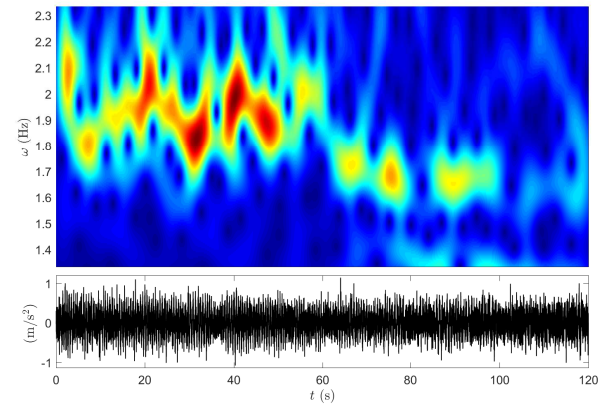
Figure 4.12: The CCWT of (a) 1st, (b) 2nd, (c) 3rd, and (d) 4th modes under Case 3
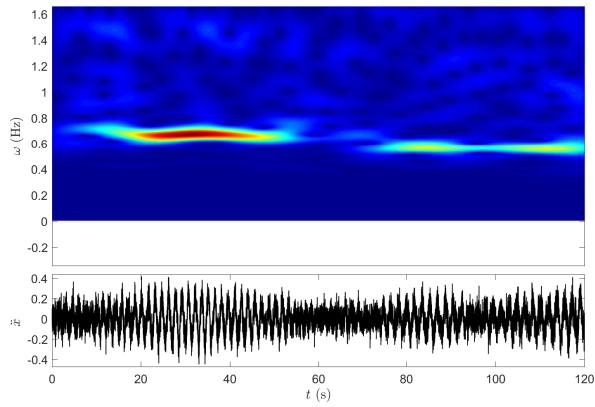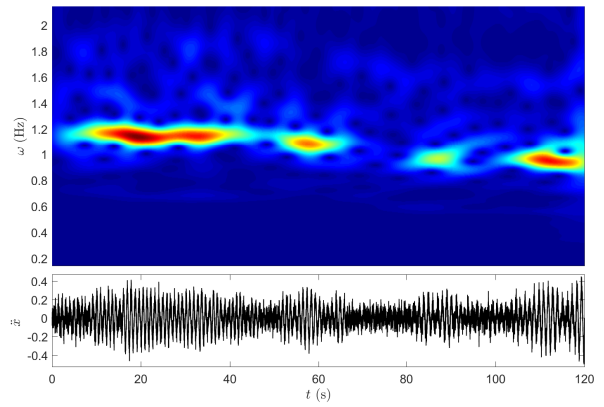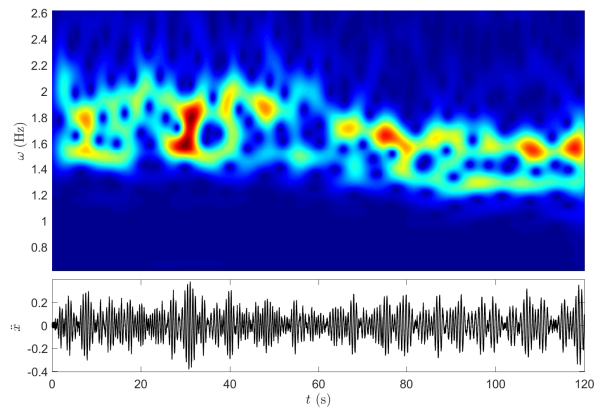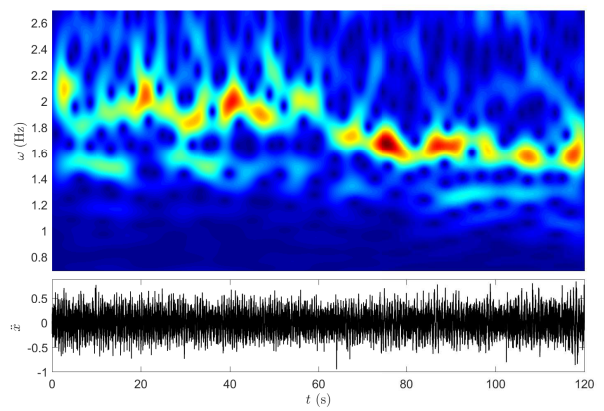
Figure 4.13: The CCWT of (a) 1st, (b) 2nd, (c) 3rd, and (d) 4th modes under Case 4

Figure 4.14: Experimental model

Table 4.2: Changes of frequencies under different damage scenarios

Mode	Undamaged	Case 1	Case 2	Case 3	Case 4
1	0.67	0.58	0.58	0.57	0.56
2	1.14	1.07	1.03	0.99	0.95
3	1.53	1.47	1.33	1.31	1.28
4	1.88	1.86	1.77	1.63	1.68

three floors have a width of 96.3 mm, length of 205 mm and thickness of 16 mm. The upper three floors have a width of 95.5 mm, length of 205 mm and thickness of 8.3 mm. Diagonal bracing is placed between the lower three floors to increase the stiffness of the model. The braces are made from a high-density polyethylene (HDPE) with aluminum on front and back. To simulate progressive damage, a butane torch is directed toward the bracing to heat up the bracing slowly to reduce the material strength.

The model is mounted over a shaking table operated by a modal shaker. The modal shaker is an electrodynamic shaker system (model 2100E11) with a frequency range between 2-5400 Hz, max random force of 310 N and a stroke length of 25.4 mm. The shaker is attached to the shake table by a steel stinger. The control system is a closed loop system where the desired signal is sent from the computer through the control system (Spider 81B by Crystal Instruments) and amplifier to the shaker. To close the loop, an accelerometer is attached to the shake table base to provide feedback to the control system. The feedback signal is compared to the desired shaker drive. The control system learns from the feedback and adjusts so the shaker best follows the desired signal. Such a closed

<div align="center">a)   b)</div>
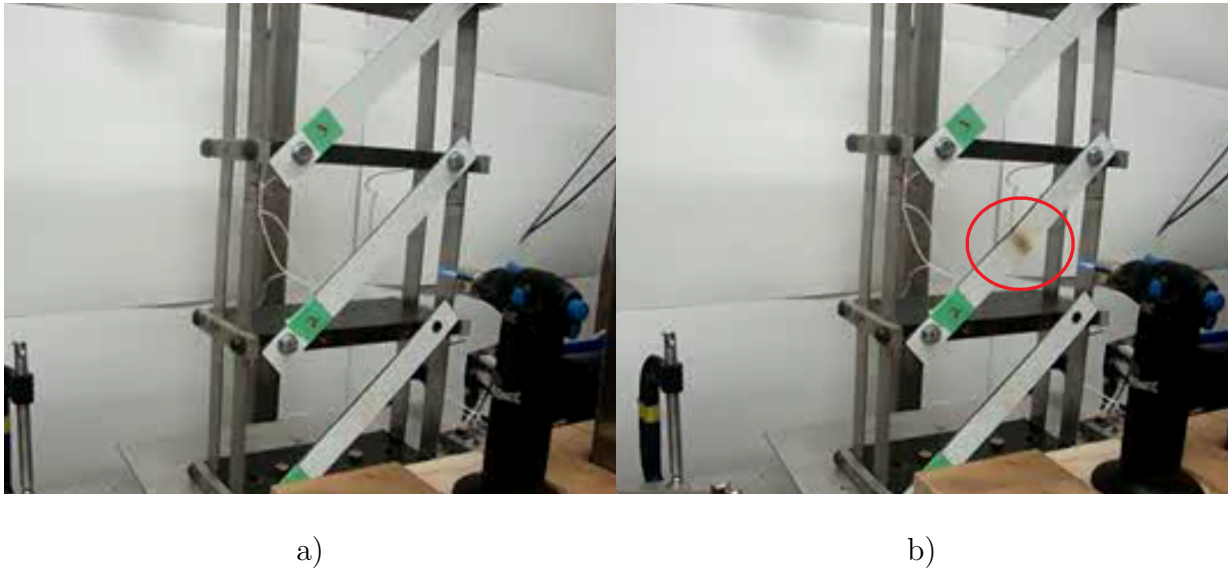
Figure 4.15: Heating of the bracing on second floor (a) before and (b) after damage

loop system improves the shaker performance and facilitates in collecting good quality of data. The vibration data is collected with ICP model 333B50 accelerometers where the sensors can measure a frequency range from 0.5 to 3000 Hz and sensitivity of 100 mV/g.

4.4.2 Test Results

During the tests, a butane torch is placed at a distance of 5 inches from the brace. It is found that a time period of approximately 50 seconds is taken for the brace to gradually loss all strength at this distance. The heat from the torch reduces the brace stiffness as the material heats up shown in Fig. 4.15. The damaged area of the braces are shown in Fig. 4.16 with a closer view.

Figure 4.17 shows the CCWT results for damage in the first floor. The results show a slight progressive frequency reduction from 40.3 Hz to 39.4 Hz starting at 38 seconds and
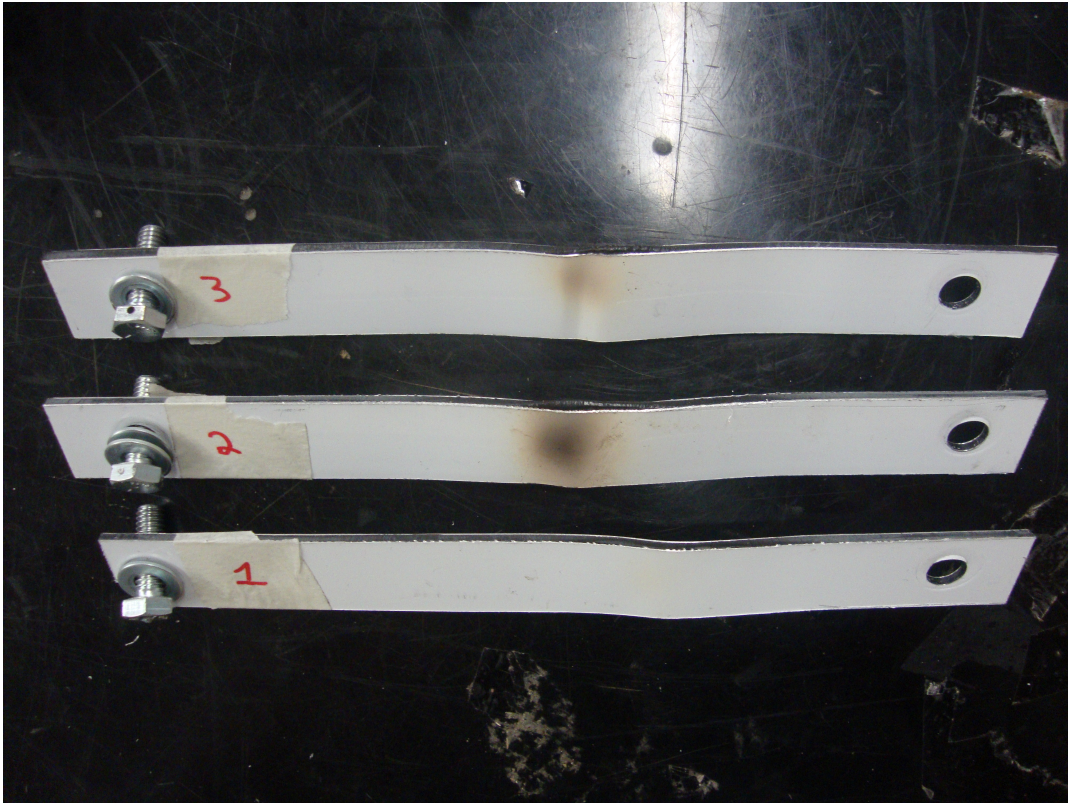
Figure 4.16: Closer view of damaged bracing
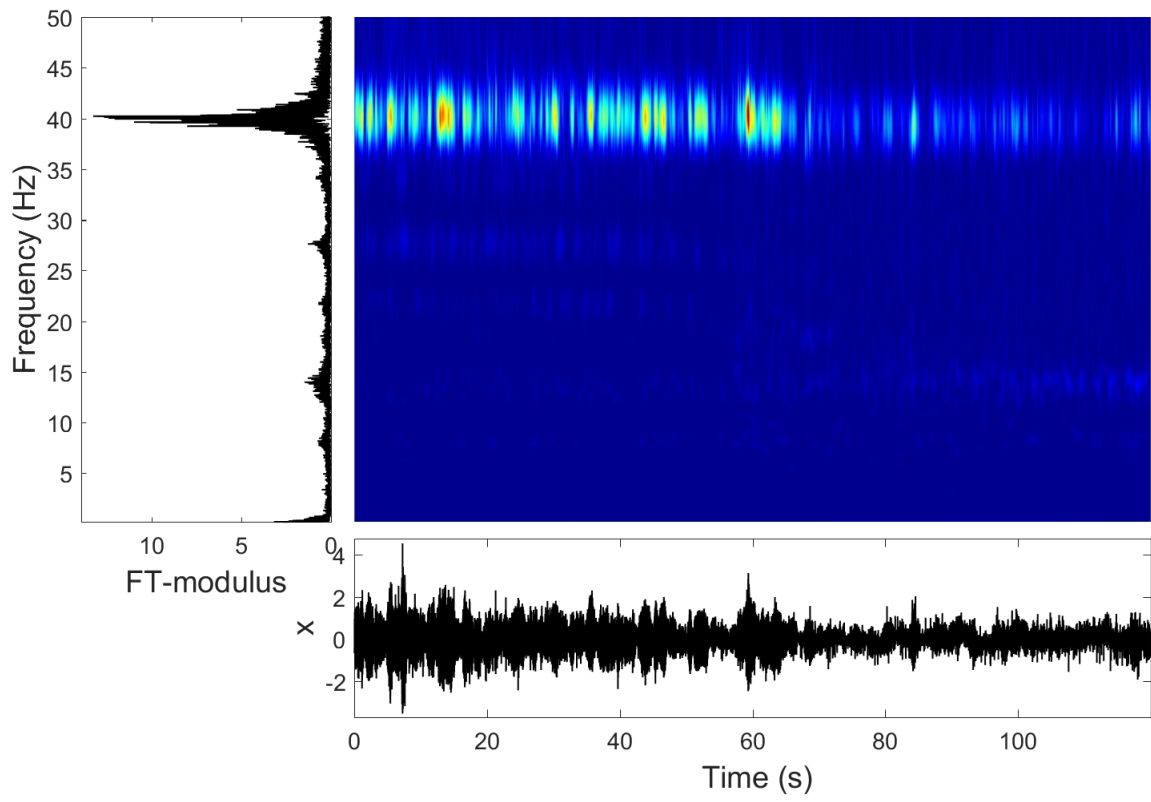
Figure 4.17: Identification results of the proposed method

continuing till 82 seconds.

Chapter 5

Conclusions and Recommendations

In this chapter, all relevant conclusions of the thesis are presented followed by the major research contributions. The potential future work are outlined next.

5.1 Key Conclusions

- The tensor decomposition-based method is explored as a robust modal identification technique under amplitude-dependent nonstationary responses. The method is validated using a suite of more than 1400 ground motions and human-induced vibrations. Such excitation covers a wide range amplitude-dependent nonstationary excitation quantified by stationary duration showing its suitability for amplitude dependent excitations. It is also observed that, with relatively moderate nonstationary data (having $\frac{T_s}{T} > 0.4$), the performance of the proposed method is accurate with least uncertainties.

- The tensor decomposition-based method is shown to perform well under various lag

parameters. This is validated with various seismic excitations. It is also shown that resolution is improved with an increase in the lag parameter.

- The tensor decomposition is found to provide accurate modal identification using a limited number of sensors. The performance of the proposed method and the associated uncertainties are discussed using limited number of sensors compared to full sensor densities. This method is validated using several numerical models and a full-scale footbridge subjected to pedestrian-induced vibration.

- A new time-frequency method is proposed by integrating the tensor decomposition with the CCWT to track the progressive changes in the structure. The proposed method is shown to have capability of separating modal responses and subsequently identifies the progressive changes in the modal parameters. This is validated using several simulation models and an experimental study where progressive damage is simulated in the bracing through a heating torch.

5.2   Contributions

The proposed research involves a combination of analytical, experimental as well as full-scale studies. This research resulted in one journal paper and two conference papers that are already published.

1. **P. Friesen** and A. Sadhu (2017). "Performance of tensor decomposition based modal identification under nonstationary vibration", *Smart Materials and Structures*, IOP, 26(3): 035024.

2. **P. Friesen** and A. Sadhu (2017). "Detection of progressive deterioration of structures using wavelet transform", *6th International Conference on Engineering Mechanics*

and Materials, CSCE Conference, Vancouver, Canada.

3. **P. Friesen** and A. Sadhu (2016). "Addressing issues of modal identification using tensor decomposition", *5th International Structural Specialty CSCE Conference*, London, Canada.

5.3   Future Work

In this thesis, an attempt is made to develop progressive damage detection method for structures. There are several areas where the current work can be further improved to make the proposed research more robust.

1. Validate the proposed method with further experiments using different damage scenarios at different locations and check the sensitivity of the method towards damage detection.

2. Incorporate damage index to identify the location of damage by utilizing the mode-shapes.

3. Achieve finer frequency resolution to capture very minor damage in the structure such that the environmental effects can be delineated.

4. The current method is able to identify the modal parameters only. It will be expanded further to identify the physical parameters (i.e., stiffness or mass) of the structures.

5. Investigate the current experimental studies with a bigger model or steel bridge under a high-capacity actuator.

6. Conduct real-time implementation of the proposed approach such that it can be applied remotely.

7. Implement the proposed methodology in several full-scale structures including bridges, dams and wind turbines.

References

[1] F. Abazarsa, S. F. Ghahari, F. Nateghi, and E. Taciroglu. Response-only modal identification of structures using limited sensors. *Structural Control and Health Monitoring*, 20(6):987–1006, 2013.

[2] F. Abazarsa, F. Nateghi, S. F. Ghahari, and E. Taciroglu. Extended blind modal identification technique for nonstationary excitations and its verification and validation. *Journal of Engineering Mechanics*, 142(2):DOI: 10.1061/(ASCE)EM.1943–7889.0000990, 04015078, 2015.

[3] G. Abbiati, R. Ceravolo, and C. Surace. Time-dependent estimators for on-line monitoring of full-scale structures under ambient excitation. *Mechanical Systems and Signal Processing*, 60-61:166–181, 2015.

[4] O. Abdeljaber and O. Avci. Nonparametric structural damage detection algorithm for ambient vibration response: Utilizing artificial neural networks and self-organizing maps. *Journal of Architectural Engineering*, 22(2):04016004, 2016.

[5] J. P. Amezquita-Sanchez and H. Adeli. Signal processing techniques for vibration-based health monitoring of smart structures. *Archives of Computational Methods in Engineering*, 23(1):1–15, 2016.

[6] Y. An, Bi. Spencer, and J. Ou. Real-time fast damage detection of shear structures with random base excitation. *Measurement*, 74:92–102, 2015.

[7] J. Antoni and S. Chauhan. An alternating least squares (ALS) based blind source separation algorithm for operational modal analysis. In *Proceedings of the 29th IMAC*, Jacksonville (FL), USA, 2011.

[8] P. Argoul and T. Le. Instantaneous indicators of structural behavior based on the continuous cauchy wavelet analysis. *Archives of Computational Methods in Engineering*, 17(1):243–250, 2003.

[9] S. Arsava, J. Chong, and Y. Kim. A novel health monitoring scheme for smart structures. *Journal of Vibration and Control*, 22(2):530–548, 2016.

[10] A. Bagheri, A. Hosseinzadeh, Pi. Rizzo, and G. Amiri. Time domain damage localization and quantification in seismically excited structures using a limited number of sensors. *Journal of Vibration and Control*, page 1077546315625141, 2016.

[11] R. Bro. Parafac: Tutorial and applications. *Chemomemcs and Intelligent Laboratory Systems*, 38:149–171, 1997.

[12] S. Cao and H. Ouyang. Robust structural damage detection and localization based on joint approximate diagonalization technique in frequency domain. *Smart Materials and Structures*, 26(1):015005, 2017.

[13] J. D. Carroll and J. J. Chang. Analysis of individual differences in multidimensional scaling via an n-way generalization of eckart-young decomposition. *Psychometrika*, 35:283–319, 1970.

[14] K. Molt K. Niemller A. Depczynski, U. Jetter. The fast wavelet transform on compact intervals as a tool in chemometrics: Ii. boundary effects, denoising and compression. *Chemometrics and Intelligent Laboratory Systems*, 49(2):151–161, 1999.

[15] P. Dharap, B. Koh, and S. Nagarajaiah. Structural health monitoring using armarkov observers. *Journal of Intelligent Material Systems and Structures*, 17(6):469–481, 2006.

[16] Y. Ding, B. Zhao, B. Wu, G. Xu, Q. Lin, H. Jiang, and Q. Miao. A condition assessment method for time-variant structures with incomplete measurements. *Mechanical Systems and Signal Processing*, 58:228–244, 2015.

[17] K. Dziedziech, W. Staszewski, and T. Uhl. Wavelet-based modal analysis for time-variant systems. *Mechanical Systems and Signal Processing*, 50:323–337, 2015.

[18] Silvano Erlicher and Pierre Argoul. Modal identification of linear non-proportionally damped systems by wavelet transform. *Mechanical Systems and signal processing*, 21(3):1386–1421, 2007.

[19] E. Figueiredo, L. Radu, K. Worden, and C. Farrar. A bayesian approach based on a markov-chain monte carlo method for damage detection under unknown sources of variability. *Engineering Structures*, 80:1 – 10, 2014.

[20] R. A. Harshman. Foundations of the PARAFAC procedure: Models and conditions for an explanatory multi-model factor analysis. *UCLA working papers in Phonetics*, 16:1–84, 1970.

[21] E. Hernandez. Identification of localized structural damage from highly incomplete modal information: Theory and experiments. *Journal of Engineering Mechanics*, 142(2):04015075, 2015.

[22] C.S. Huang, C.Y. Liu, and W.C. Su. Application of cauchy wavelet transformation to identify time-variant modal parameters of structures. *Mechanical Systems and Signal Processing*, 80:302 – 323, 2016.

[23] S. Jang, B. Spencer, and S. Sim. A decentralized receptance-based damage detection strategy for wireless smart sensors. *Smart Materials and Structures*, 21(5):055017, 2012.

[24] N. Khoa, B. Zhang, Y. Wang, F. Chen, and S. Mustapha. Robust dimensionality reduction and damage detection approaches in structural health monitoring. *Structural Health Monitoring*, page 1475921714532989, 2014.

[25] Y. Kim, J. Chong, K. Chon, and J. Kim. Wavelet-based ar–svm for health monitoring of smart structures. *Smart Materials and Structures*, 22(1):015003, 2012.

[26] A. Klepka and T. Uhl. Identification of modal parameters of non-stationary systems with the use of wavelet based adaptive filtering. *Mechanical Systems and Signal Processing*, 47(1):21–34, 2014.

[27] J. B. Kruskal. Three-way arrays: rank and uniqueness of trilinear decompositions with applications to arithmetic compexity and statistics. *Linear Algebra and its application*, 18:95–138, 1977.

[28] L. D. Lathauwer and J. Castaing. Blind identification of underdetermined mixtures by simultaneous matrix diagonalization. *IEEE Transactions on Signal Processing*, 56(3):1096–1105, 2008.

[29] Le, Quang Tuyen, Huang, Chiung Shiann, and Su, Wei Chih. Application of damage locating vectors approach on monitoring shock isolation system. *MATEC Web Conf.*, 71:04006, 2016.

[30] Le, Thien-Phu and Argoul, Pierre. Continuous wavelet transform for modal identification using free decay response. *Journal of sound and vibration*, 277(1):73–100, 2004.

[31] C. C. Lin, C. M. Hu, J. F. Wang, and R. Y. Hu. Vibration control effectiveness of passive tuned mass dampers. *Journal of the Chinese Institute of Engineers*, 17:367–376, 1994.

[32] R. Link and D. Zimmerman. Structural damage diagnosis using frequency response functions and orthogonal matching pursuit: theoretical development. *Structural Control and Health Monitoring*, 22(6):889–902, 2015.

[33] Gang Liu, Zhu Mao, and Michael Todd. Damage detection using transient trajectories in phase-space with extended random decrement technique under non-stationary excitations. *Smart Materials and Structures*, 25(11):115014, 2016.

[34] T. Ma, H. Yang, and C. Chang. Structural damage diagnosis and assessment under seismic excitations. *Journal of engineering mechanics*, 131(10):1036–1045, 2005.

[35] N. M. M. Maia and J. M. M. Silva. Modal analysis identification techniques. *Philolophical transactions of the royal society*, 359(1778):29–40, 2001.

[36] S. I. Mcneill. Extending blind modal identification to the underdetermined case for ambient vibration. In *ASME 2012 International Mechanical Engineering Congress and Exposition*, pages 241–252, Houston, Texas, USA, November, 2012, 2012.

[37] K. Mokios, N. D. Sidiropoulos, and A. Potamianos. Blind speech separation using PARAFAC analysis and integer least squares. *Proceedings of ICASSP'06*, 5:73–76, 2006.

[38] M. Mollineaux and R. Rajagopal. Structural health monitoring of progressive damage. *Earthquake Engineering & Structural Dynamics*, 44(4):583–600, 2015.

[39] M. Munoz, P. Argoul, and F. Farges. Continuous cauchy wavelet transform analyses of exafs spectra. a qualitative approach. *American Mineralogist*, 88:694–700, 2003.

[40] F. Musafere, A. Sadhu, and K. Liu. Towards damage detection using blind source separation integrated with time-varying auto-regressive modeling. *Smart Materials and Structures*, 25(1):015013, 2015.

[41] S. Panigrahi, S. Chakraverty, and B. Mishra. Damage identification of multistory shear structure from sparse modal information. *Journal of Computing in Civil Engineering*, 27(1):1–9, 2011.

[42] C. Papadimitriou, J. L. Beck, and S. K. Au. Entropy-based optimal sensor location for structural model updating. *Journal of Vibration and Control*, 6:781–800, 2000.

[43] A. Sadhu, A. Goldack, and S. Narasimhan. Ambient modal identification using multi-rank parallel factor decomposition. *Structural Control and Health Monitoring*, 22(4):595–614, 2015.

[44] A. Sadhu and B. Hazra. A novel damage detection algorithm using time-series analysis-based blind source separation. *Shock and Vibration*, 20(3):423–438, 2013.

[45] A. Sadhu, B. Hazra, and S. Narasimhan. Decentralized modal identification of structures using parallel factor decomposition and sparse blind source separation. *Mechanical Systems and Signal Processing*, 41(1-2):396–419, 2013.

[46] A. Sadhu, B. Hazra, and S. Narasimhan. Ambient modal identification of structures equipped with tuned mass dampers using parallel factor blind source separation. *Smart Structures and Systems*, 13(2):257–280, 2014.

[47] Goldack A. Sadhu, A. and S. Narasimhan. Decentralized modal identification of a pony truss pedestrian bridge using wireless sensors. *Journal of Bridge Engineering*, 19(6):04014013, 2014.

[48] A. Smilde, R. Bro, and P. Geladi. *Multi-way Analysis with Applications in the Chemical Sciences*. John Wiley and Sons, Ltd, West Sussex, UK, 2004.

[49] C. Su, W. Liao, L. Tan, and R. Chen. Reliability-based damage identification using dynamic signatures. *Journal of Bridge Engineering*, 21(3):04015058, 2016.

[50] Wei C. Su, Tuyen Q. Le, Chiung S. Huang, and Pei Y. Lin. Locating damaged storeys in a structure based on its identified modal parameters in cauchy wavelet domain. *Applied Mathematical Modelling*, 2017.

[51] Z. Sun and C. Chang. Statistical wavelet-based method for structural health monitoring. *Journal of structural engineering*, 130(7):1055–1062, 2004.

[52] G. Tondreau and A. Deraemaeker. Automated data-based damage localization under ambient vibration using local modal filters and dynamic strain measurements: Experimental applications. *Journal of Sound and Vibration*, 333(26):7364 – 7385, 2014.

[53] M.D. Trifunac and A.G. Brady. A study on the duration of strong earthquake ground motion. *Bulletin of the Seismological Society of America*, 65(3):581–626, 1975.

[54] M. Ulriksen and L. Damkilde. Structural damage localization by outlier analysis of signal-processed mode shapes analytical and experimental validation. *Mechanical Systems and Signal Processing*, 6869:1 – 14, 2016.

[55] J. Valdés-González, J. De-la Colina, and C.A. González-Pérez. Experiments for seismic damage detection of a rc frame using ambient and forced vibration records. *Structural Control and Health Monitoring*, 22(2):330–346, 2015.

[56] R. Villaverde and L. A. Koyama. Damped resonant appendages to increase inherent damping in buildings. *Earthquake Engineering and Structural Dynamics*, 22(6):491–507, 1993.

[57] J.H. Weng and C.H Loh. Recursive subspace identification for on-line tracking of structural modal parameter. *Mechanical Systems and Signal Processing*, 25(8):2923 – 2937, 2011.

[58] L. Yu and J.H. Zhu. Structural damage prognosis on truss bridges with end connector bolts. *Journal of Engineering Mechanics*, 0(0):B4016002, 0.

[59] Kaihui Zhong and C. C. Chang. Recursive combined subspace identification technique for tracking dynamic characteristics of structures under earthquake excitation. *Journal of Engineering Mechanics*, 142(12):04016092, 2016.

APPENDICES

Appendix A

Alternating least square

Alternating least square (ALS) is mainly comprised of the following key steps to undertake simultaneous unfolding of three model matrices [11]:

1. Keeping $\boldsymbol{\theta}$ and $\boldsymbol{\phi}$ same, $\boldsymbol{\psi}$ is solved using:

$$\min_{\boldsymbol{\psi}} \|\bar{\mathbf{S}} - [[\boldsymbol{\theta}, \boldsymbol{\phi}, \boldsymbol{\psi}]]\|^2 \equiv \min_{\boldsymbol{\psi}} \|\bar{\mathbf{S}}_{(3)} - \boldsymbol{\psi}(\boldsymbol{\phi} \odot \boldsymbol{\theta})^T\|^2 \qquad (A.1)$$

where $\odot$ represents Khatri-Rao product. Given $\boldsymbol{\theta}\epsilon\Re^{I \times R}$ and $\boldsymbol{\phi}\epsilon\Re^{J \times R}$, then $\boldsymbol{\theta} \odot \boldsymbol{\phi}$ is

a matrix with IJ rows and R columns and is expressed as:

$$\boldsymbol{\theta} \odot \boldsymbol{\phi} = \begin{bmatrix} \theta_{11} & \theta_{12} & \cdots\cdots & \theta_{1R} \\ \theta_{21} & \theta_{22} & \cdots\cdots & \theta_{2R} \\ \vdots & \vdots & \cdots\cdots & \vdots \\ \theta_{I1} & \theta_{I2} & \cdots\cdots & \theta_{IR} \end{bmatrix} \odot \begin{bmatrix} \phi_{11} & \phi_{12} & \cdots\cdots & \phi_{1R} \\ \phi_{21} & \phi_{22} & \cdots\cdots & \phi_{2R} \\ \vdots & \vdots & \vdots & \vdots \\ \phi_{J1} & \phi_{J2} & \cdots\cdots & \phi_{JR} \end{bmatrix}$$

$$= \begin{bmatrix} \theta_{11}\phi_{:1} & \theta_{12}\phi_{:2} & \cdots\cdots & \theta_{1R}\phi_{:R} \\ \theta_{21}\phi_{:1} & \theta_{22}\phi_{:2} & \cdots\cdots & \theta_{2R}\phi_{:R} \\ \vdots & \vdots & \vdots & \vdots \\ \theta_{I1}\phi_{:1} & \theta_{I2}\phi_{:2} & \cdots\cdots & \theta_{IR}\phi_{:R} \end{bmatrix}$$

where $\phi_{:k}$ represents k-th column of $\boldsymbol{\phi}$.

2. Optimal $\boldsymbol{\psi}$ is the least square solution which can be obtained using:

$$\boldsymbol{\psi} = \bar{\mathbf{S}}_{(3)}(\boldsymbol{\phi} \odot \boldsymbol{\theta})(\boldsymbol{\phi}^T\boldsymbol{\phi} * \boldsymbol{\theta}^T\boldsymbol{\theta})^\dagger. \tag{A.2}$$

3. Then each component of $\boldsymbol{\theta}$, $\boldsymbol{\phi}$ and $\boldsymbol{\psi}$ are solved until the desired convergence is achieved:

$$\boldsymbol{\theta} \longleftarrow \bar{\mathbf{S}}_{(1)}(\boldsymbol{\psi} \odot \boldsymbol{\phi})(\boldsymbol{\psi}^T\boldsymbol{\psi} * \boldsymbol{\phi}^T\boldsymbol{\phi})^\dagger$$

$$\boldsymbol{\phi} \longleftarrow \bar{\mathbf{S}}_{(2)}(\boldsymbol{\psi} \odot \boldsymbol{\theta})(\boldsymbol{\psi}^T\boldsymbol{\psi} * \boldsymbol{\theta}^T\boldsymbol{\theta})^\dagger$$

$$\boldsymbol{\psi} \longleftarrow \bar{\mathbf{S}}_{(3)}(\boldsymbol{\phi} \odot \boldsymbol{\theta})(\boldsymbol{\phi}^T\boldsymbol{\phi} * \boldsymbol{\theta}^T\boldsymbol{\theta})^\dagger. \tag{A.3}$$

Finally, the ALS estimates a tensor $\hat{\bar{\mathbf{S}}} = \sum_{\mathbf{r=1}}^{\mathbf{R}} \boldsymbol{\theta_r} \circ \boldsymbol{\phi_r} \circ \boldsymbol{\psi_r}$ such that the following objective function is minimized:

$$f(\boldsymbol{\theta}, \boldsymbol{\phi}, \boldsymbol{\psi}) = \|\bar{\mathbf{S}} - \hat{\bar{\mathbf{S}}}\|^2. \tag{A.4}$$

A unique decomposition can be obtained if the Kruskal condition [27] is satisfied:

$$l_{\boldsymbol{\theta}} + l_{\boldsymbol{\phi}} + l_{\boldsymbol{\psi}} \geq 2R + 2 \tag{A.5}$$

where $l_{\boldsymbol{\theta}}$, $l_{\boldsymbol{\phi}}$ and $l_{\boldsymbol{\psi}}$ are l-rank of the matrices $\boldsymbol{\theta}$, $\boldsymbol{\phi}$ and $\boldsymbol{\psi}$ respectively, where l-rank is defined as maximum number l such that each set of l columns of the matrix is linearly independent.

Appendix B

Details of the 5-DOF model

The 5-DOF model used in this paper is taken from [31]. Following are the mass, damping, and stiffness matrices of the 5-DOF model.

$$
M(Ns^2/cm) = \begin{bmatrix} 19.57 & 0 & 0 & 0 & 0 \\ 0 & 19.57 & 0 & 0 & 0 \\ 0 & 0 & 19.57 & 0 & 0 \\ 0 & 0 & 0 & 19.57 & 0 \\ 0 & 0 & 0 & 0 & 19.57 \end{bmatrix} \tag{B.1}
$$

$$
C(Ns/cm) = \begin{bmatrix} 47.19 & -13.67 & -0.79 & 0.30 & 0.06 \\ & 37.46 & -15.61 & -1.04 & 0.46 \\ & & 36.22 & -16.46 & 0.11 \\ & sym. & & 34.26 & -14.28 \\ & & & & 15.93 \end{bmatrix} \tag{B.2}
$$

$$K(N/cm) = \begin{bmatrix} 77108 & -36564 & 4549 & 1612 & -211 \\ & 58596 & -35825 & 5481 & 1169 \\ & & 58344 & -36587 & 7463 \\ & sym. & & 52688 & -22962 \\ & & & & 14621 \end{bmatrix} \quad \text{(B.3)}$$